COMPUTATIONAL ANALYSIS OF PROGNOSIS OF MYOCARDIAL INFARCTION IN LEFT VENTRICLE
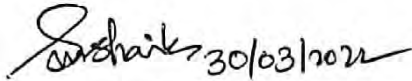
by

Md. Tofazzal Hossain

A thesis submitted in partial fulfillment of the requirements for the degree of

MASTER OF SCIENCE IN MECHANICAL ENGINEERING

Department of Mechanical Engineering

BANGLADESH UNIVERSITY OF ENGINEERING AND TECHNOLOGY
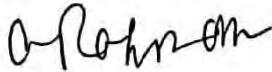
Dhaka, Bangladesh

March 2022

The thesis titled "COMPUTATIONAL ANALYSIS OF PROGNOSIS OF MYOCARDIAL INFARCTION IN LEFT VENTRICLE" submitted by Md. Tofazzal Hossain, Roll No.: 0419102029, Session: April, 2019, has been accepted as satisfactory in partial fulfillment of the requirement for the degree of MASTER OF SCIENCE IN MECHANICAL ENGINEERING on March 30, 2022.
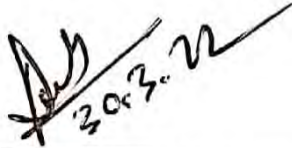
BOARD OF EXAMINERS

Dr. Sheikh Mohammad Shavik
Assistant Professor
Department of Mechanical Engineering,
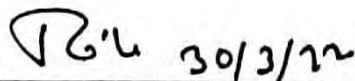BUET, Dhaka- 1000

Chairman
(Supervisor)

Dr. Muhammad Ashiqur Rahman
Professor and Head
Department of Mechanical Engineering,
BUET, Dhaka- 1000

Member
(Ex-officio)

Dr. Mohammad Abdul Motalab
Professor
Department of Mechanical Engineering,
BUET, Dhaka- 1000

Member

Dr. Muhammad Tarik Arafat
Associate Professor
Department of Biomedical Engineering,
BUET, Dhaka- 1000

Member
(External)

CANDIDATE'S DECLARATION

It is hereby declared that this thesis or any part of it has not been submitted elsewhere for the award of any degree or diploma.

March 2022

Md. Tofazzal Hossain
Author

CERTIFICATE OF RESEARCH

This is to certify that the work presented in this thesis has been carried out by the author under the supervision of **Dr. Sheikh Mohammad Shavik**, Assistant Professor, Department of Mechanical Engineering, Bangladesh University of Engineering and Technology, Dhaka.

<table>
<tr><td>_____</td><td></td><td>_____</td></tr>
<tr><td>**Dr. Sheikh Mohammad Shavik**</td><td></td><td>**Md. Tofazzal Hossain**</td></tr>
</table>

DEDICATION

Dedicated to My Spouse and Daughter

TABLE OF CONTENTS

LIST OF FIGURES

LIST OF TABLES

ACKNOWLEDGEMENT

I would like to express my deepest gratitude and indebtedness to my supervisor **Dr. Sheikh Mohammad Shavik**, Assistant Professor, Department of Mechanical Engineering, BUET, for his kind supervision, constant guidance, encouragement, support, and thoughtful discussion throughout the entire research. Without his guidance, it was impossible to complete the thesis work.

I wish to thank my parents, spouse, colleagues, and well-wishers for their help and mental support during the research.

Finally, I wish to thank the Almighty Allah (SWT) for everything in my entire life.

Author

ABSTRACT

Heart Failure due to Acute Myocardial Infarction (HF AMI) has emerged as prevalent heart disease with a high risk of short-term and long-term mortality rates. HF AMI has been associated with a progressively impaired interaction between the left ventricle (LV) and the systemic arteries. The progression of HF AMI and the key factors contributing to this process is an area of active research. Since the structural and functional changes of the Left Ventricle (LV) govern the progression of HF AMI, computational models have emerged as a robust tool to study the features of HF AMI and develop an effective treatment plan in recent years. FE model of LV would help assess the contributions of the critical factors to the progression of HF AMI. In the present study, a coupled LV FE-lumped parameter circulatory modelling framework has been calibrated with the measurements acquired from literature for a healthy subject and HF AMI patient. Both the healthy and HF AMI case models reproduced the literature datasets within acceptable limits. After that, the HF AMI model parameters such as geometry (Infarct Size: 9% to 27% of healthy LV volume, and Infarct Location: -3.5 cm to -5.5 cm), stiffness (up to 24% of healthy LV stiffness have been increased), and contractility (up to 30% of healthy LV contractility have been decreased) were varied to reproduce the effects of these parameters on the progression of HF AMI. The model predicts key features of HF AMI progression. The increase in infarct size produced a reduction in ejection fractions accompanied by a decrease in peak circumferential, longitudinal, and radial strains. Similar outcomes have been found by shifting the infract zone location towards the base of the LV (case: $z = -3.5$ cm). At the extreme basal location of infarct zone ($z = -3.5$ cm) with 9% of left ventricle volume (LVV) infarct size, the LV's dysfunction behaves like the extreme infarct size of 27% of LVV located at the mid-plane. The increase in infarct size increases the stiffness and reduces the contractility of LV. While isolated variations in these parameters have been shown to contribute to the severity of HF AMI, multiple mechanisms must likely be combined to reproduce all the pathophysiological features observed during the progression of HF AMI.

CHAPTER 1

INTRODUCTION

Thirty percent of the world's deaths are attributed to cardiovascular disease, the most prevalent cause of mortality worldwide. Coronary artery disease and stroke account for more than 75% of these deaths [1]. Tobacco use, being overweight, having high cholesterol or blood pressure are all the risk factors for heart disease. These cardiovascular disorders might range from mild chest discomfort and shortness of breath to more severe chest pain and breathlessness. When diagnosing heart failure (HF), ejection fraction, or the proportion of blood expelled from the left ventricle (LV) with each pulse, is employed as a clinical indication to diagnose HF.

The blood circulatory system is made up of pulmonary and systemic circuits. Two ventricles and two atria make up the human heart's muscular chambers. Heart pumps are separated into two parts: one for each side of the body (left and right). The systemic and pulmonary circuits are connected to the heart's left and right chambers, respectively. The LV and left atrium (LA) pump oxygen-rich blood through the circulatory system in the left heart. Oxygen-depleted blood flows to the right lungs through the right ventricle (RV) and right atrium (RA) (see Figure 1.1) [2].

Sudden blockage or cut-off of the blood supply is described as "heart attack." It is possible that a myocardial infarction (MI) may go unnoticed for an extended period or that it may lead to hemodynamic worsening and even death. Many heart attacks are caused by coronary artery disease (CAD), the common cause of mortality. When the coronary artery (CA) is completely blocked, the heart's myocardium is starved of oxygen.

MI and CAD are closely linked. An international multicenter case-control study, INTERHEART, identified the following modifiable coronary artery disease risk factors: depression, global stress, financial stress, and life events are all associated with an increased risk of cardiovascular disease and other chronic illnesses. Except for excessive alcohol consumption, all of the above risk factors were significantly linked to an acute myocardial infarction in the INTERHEART study. Drugs, smoking, cold weather, and extreme stress trigger the progression of acute myocardial infarction (AMI). Myocardial necrosis occurs as a result of prolonged ischemia. The necrosis progresses from the sub-endocardium to the sub-epicardium [3]. Infarction heals via tissue injury, heart dilatation, and cardiac dysfunction due

to the myocardium's inability to regenerate [4]. Sweating, chest pain, upper extremity pain, and stomach discomfort can all be symptoms of AMI [5]. The MI can appear in various ways, including palpitations and cardiac arrest. In addition, there are situations when the MI does not show any symptoms [7].

Source: https://byjus.com/biology/double-circulation/
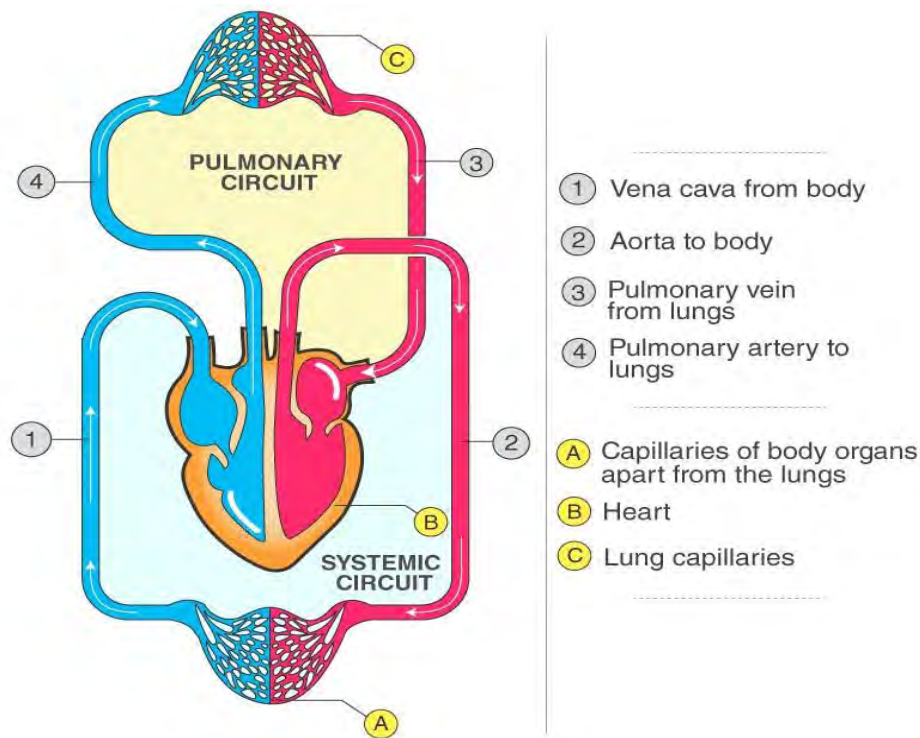
Figure 1. 1: Human heart blood circulation circuits

The LV is commonly affected by MI, however, injury to RV or the atria can also occur, known as RV infarction. RV infarction accompanied by LV infarction greatly raises the risk of death. There is a worse prognosis for anterior infarcts since they are more extensive and more widespread. These infarcts are frequently caused by blockage of the left coronary artery, especially in its anterior portion [7]. Computer heart models that accurately depict cardiac geometry and muscle architecture have come a long way in recent years [8]. The computer model prompts the researchers to explore the underlying causes of cardiovascular disorders that are not possible to study in a clinical context. Despite these substantial achievements, some unsolved concerns and features still require development. Understanding the mechanics of AMI is one of the objectives of this work.

In this study, we have used finite element model (FEM) to examine the MI's location and size impact on the LV's function. According to our understanding, only a small amount of study has been done on MI, which adversely impacts the LV's function. In most circumstances, it is impossible to isolate the effects of single parameter on LV's function in clinical settings; hence a computer model of the heart can help to gain more insights on determining the effects of infarct size and location on the function of LV.

1.1 Human Heart Anatomy in Brief

The heart is a muscular pump connected to the rest of the body's circulatory systems and the lungs. The heart is divided into four unique muscular chambers: two atria and two ventricles (Figure 1.2). Through the LA and LV, blood flows from the pulmonary veins to the aorta. Hundreds of millions of cardiac muscle cells (myocytes) are connected end to end at their gap junctions to form a network of muscle fibers that wrap tightly around the chamber [9]. The right heart is composed of an atrium and a ventricle which transports blood from the vena cavae to the lung arteries. Both chambers share the interventricular septum that divides the right and left ventricles. Unlike the heart, which has a robust muscular wall, the atria have thin walls and supply blood via low-pressure veins. The right tricuspid and the left mitral valves separate the atrium from the corresponding ventricles, respectively, which allows unidirectional flow only. The free ends of these valves are connected to the ventricular walls via fibrous rings known as chordae tendinae [2].

The aortic and pulmonary valves isolate each ventricle from its related artery connection to preserve unidirectional blood flow. The amount of the pressure differential across the valves dictates whether they are opened or closed. The cardiovascular system is comprised of the heart and lungs connected in a closed loop [10].
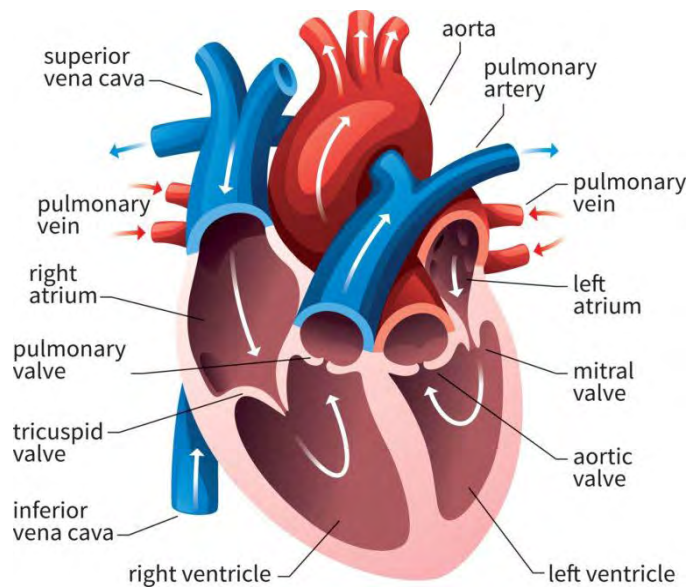
Figure 1. 2: Simplified structure of the human heart and direction of blood flow through the heart chambers and heart valves

The circulatory system carries oxygen from the air we breathe to all of our body's cells, and the lungs are supplied with oxygen-rich blood by a single pair of blood veins [10]. The pulmonary circulatory system of the lungs transports blood between the heart and lungs (Figure 1.1 and Figure 1.2). It transports deoxygenated blood to the lungs for re-oxygenation to receive oxygen and expel carbon dioxide. The oxygenated blood returns to the heart and then to the lungs. The heart initiates systemic circulation by pumping oxygenated blood into the aorta from the left ventricle [11]. After giving oxygen and nutrients to cells throughout the body, the blood returns deoxygenated blood to the RA of the heart. After oxygenation, blood moves from the LA to the LV below to re-establish systemic circulation. Both the circulatory and respiratory systems work together in harmony to maintain enough oxygenation of the body and to remove waste materials [12]. There is a balance between CO2 emission and O2 absorption. Then, oxygenated blood moves via venules from the capillary beds to the pulmonary veins [14]. The aorta, the body's largest artery, receives oxygenated blood from the LV of the heart. Systemic veins supply the prominent bodily veins known as the inferior and superior venae cavae. The venae cavae supply deoxygenated blood to the heart's right atrium (see Figure 1.3) [13].
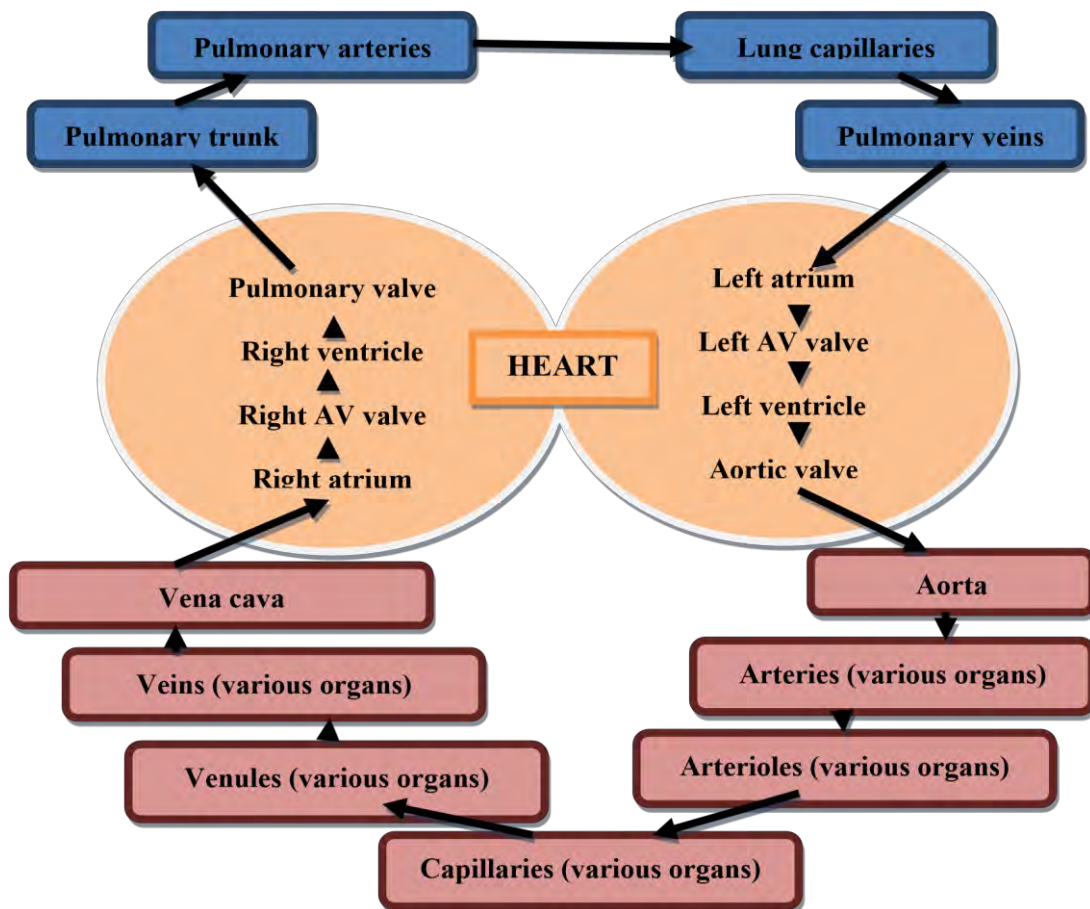
Figure 1. 3: Circulatory pathway of the cardiovascular system during systemic and pulmonary circulation [15].

Each cardiac cycle consists of a diastolic phase (relaxation) and a systolic phase (contraction). Both the atria and ventricles alternate between systole and diastole stages. In other words, the ventricles are in systole when the atria are in diastole, and vice versa [9]. Figure 1.4 depicts the phases of the cardiac cycle. Blood enters the right atrium via the superior and inferior vena cava and the left atrium via the pulmonary veins during atrial diastole. The atrioventricular valves are closed during the early stages of this phase, and blood accumulates in the atria. At some point, the pressure in the atrium exceeds the pressure in the corresponding ventricle on the same side, which opens those valves [15]. During the systolic phase, electrical depolarization causes contraction of the atria, which forces the blood from the upper chambers into lower chambers. Atrial contraction results in a further rise in atrial pressures [15-17].
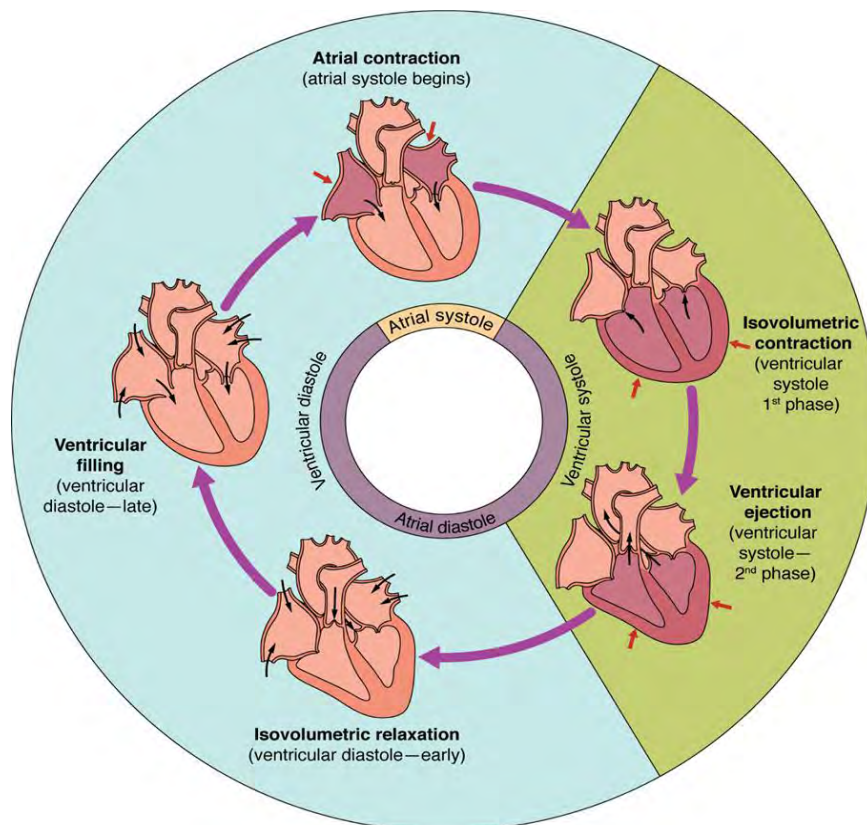
Figure 1. 4: Cardiac Cycle Overview: Atrial systole initiates the cardiac cycle, which proceeds through ventricular systole, atrial diastole, and ventricular diastole before repeating the process. The electrocardiogram (ECG) correlations are highlighted.

The pressure and volume change over time at different components (aorta, ventricles, and atriums) and electrical activity of the heart can be illustrated by using Wiggers diagrams as shown in Figure 1.5. The ventricle's pressure is subsequently delivered to the aorta. Due to the aorta's strong elasticity, its walls can dilate to handle the abrupt, drastic increase in pressure [17]. The first and greatest wave depicts these pressure variations on the aortic pressure graph. The corresponding pressure-volume relationship of LV has been depicted in Figure 1.6. Physiologically significant factors and variables can be derived via PV loop analysis. Point A indicates the end-diastolic volume (EDV), and point B measures the end-systolic volume (ESV). The peak point of the PV loop is the systolic blood pressure (SBP) can be measured from the end-systolic pressure-volume relationship (ESPVR), and the ventricular filling may be seen along with the end-diastolic pressure-volume relationship (EDPVR) [18].
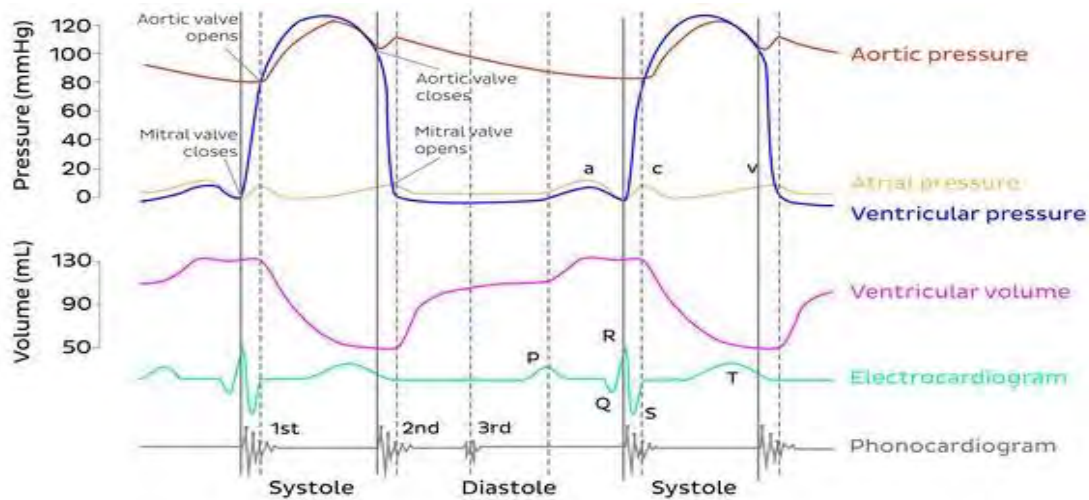
Figure 1. 5: Wiggers diagram showing aortic, left atrial, left ventricular pressure; left ventricular volume; electrocardiogram; phonocardiogram with respect to heart cycle time [4].
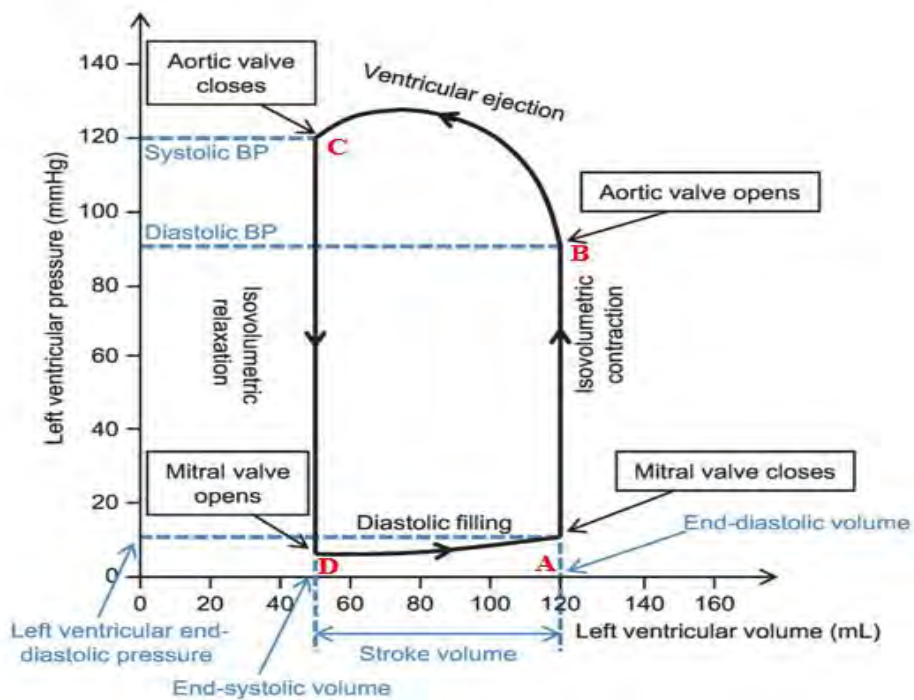
Figure 1. 6: A typical pressure – volume (PV) loop with identifiable physiological parameters, and ESPVR and EDPVR

Ventricular function is closely linked to the concepts of contractility, preload, and afterload. Contractility refers to the ability of the heart muscle to contract that generates forces during the contraction. Changes to the excitation-contraction coupling mechanism by

increasing calcium release might affect myocardial contractility. An indication of contractility known as the end-systolic elastance (Ees), fluctuates with the ventricular contractility but is not affected by changes in the artery system (afterload and preload) (Figure 1.10 a). Before contraction occurs, the myocardial wall experiences hemodynamic stress or stretch known as preload [2].
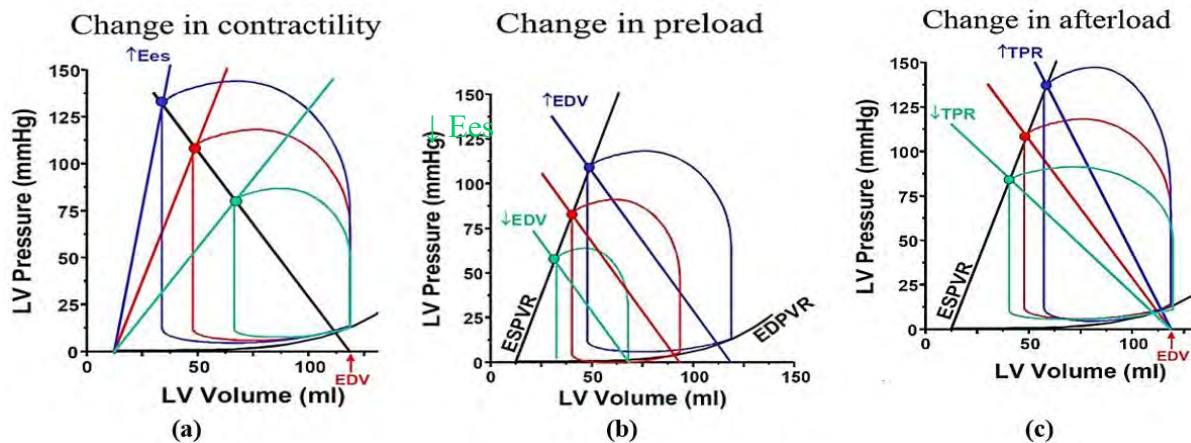
Figure 1. 7: Effect of change in (a) contractility, (b) preload, and (c) afterload on PV loop over single cardiac cycle [2].

1.2 Heart Failure and Ejection Fraction

The ejection fraction measures blood flow in the left ventricle (or right ventricle) (EF). Every time the left ventricle contracts, the amount of blood it pumps is the EF (ejection fraction). The left ventricle is the heart's major pumping chamber. A common way of measuring EF is using an EDV (end-diastolic volume). The lower the EF, the more likely the heart is to fail. The severity of an individual's EF can be used to determine if they have heart failure with reduced ejection fraction (HFrEF). Every time the heart beats, the left ventricle (the heart's major pumping chamber) expels some blood into the body. Percentage of blood pumped from the ventricle to lungs for oxygenation. "Ejection fraction" is commonly used to describe the percentage of the left ventricle that pumps blood out of the heart. Echocardiogram (ECG), magnetic resonance imaging (MRI) scan of the heart, and nuclear medicine scan or multiple gated acquisition (MUGA) of the heart, often known as a nuclear stress test, are some of the clinical methods for measuring the EF. When it comes to measuring the EF, ECG is the most popular approach. Heart health or illness can be determined by an individual's Ejection Fraction (EF). Heart failure is a condition in which the heart's pumping capacity is less than optimal. Normal blood flow in the heart is defined as between 55% and 70%. This means that

65% of the left ventricle's blood volume is pumped out the body with each pulse, as an example. The EF of a patient might change widely depending on the severity of their cardiac condition and the efficacy of their medicine [21].

- Ejection Fraction (EF) %: 55% to 70%
    - ✓ Pumping Ability of the Heart: Normal
    - ✓ Level of Heart Failure/Effect on Pumping: Heart function may be normal or may have heart failure with preserved EF (HFpEF).
- Ejection Fraction (EF) %: 40% to 54%
    - ✓ Pumping ability of the heart: Slightly below normal
    - ✓ Level of heart failure/effect on pumping: less blood is available, so less blood is ejected from the ventricles. A lower-than-normal amount of oxygen-rich blood is available to the rest of the body. The patient may not have symptoms then.
- Ejection Fraction (EF) %: 35% to 39%
    - ✓ Pumping ability of the heart: Moderately below normal
    - ✓ Level of heart failure/effect on pumping: Mild heart failure with reduced EF (HFrEF).
- Ejection Fraction (EF) %: Less than 35%
    - ✓ Pumping ability of the heart: Severely below normal
    - ✓ Level of heart failure/effect on pumping: Moderate-to-severe HFrEF. Severe HFrEF increases the risk of life-threatening heartbeats and cardiac dyssynchrony/desynchronization (right and left ventricles do not pump in unison).

Those who suffer from heart failure due to left ventricular dysfunction must see their doctors frequently to check their improvement. Depending on the underlying reason, a pacemaker or an implanted cardiac defibrillator may be required. Heart resynchronization treatment and contractility modulation can help certain moderate to severe heart problems patients. An assist device for either the left or right ventricle may be essential in cases where other therapies have failed. Heart failure is a common, costly, and sometimes dangerous disease. Only 2% of adults suffer heart failure; this climbs to 6–10% when over 65. It is projected that rates will rise. About one-third of those diagnosed die during the first year of their diagnosis; however, this percentage lowers to less than 10% by the second year [1]. An

overworked ventricle might cause a failing heart to contract weaker. There is an increase in cardiac output due to increased ventricular filling and contraction force. In heart failure patients, this mechanism begins to malfunction, resulting in less efficient cardiac muscle contractions resulting from dilated ventricles. In the past, a method of diagnosing heart failure based on the side of the heart affected was utilized (right heart failure versus left heart failure). Right, and left heart failure were formerly thought to impact the lungs and the aorta simultaneously, resulting in systemic circulatory problems that included brain and nervous system damage. Symptoms of both right and left heart failure are common in many people. Ejection fraction, the amount of blood pumped out of the heart during a single contraction, can be used to classify a patient's type of heart failure properly. EF is calculated by dividing EDV by stroke volume (SV), the proportion of EDV that is evacuated every beat [22].

$$EF(\%) = \frac{SV}{EDV} \times 100\%$$

Where the stroke volume is given by, SV= EDV – ESV

HFrEF (heart failure with reduced ejection fraction) is one of the two types of heart failure. Ejection fraction < 40% is a symptom of HFrEF. When the left ventricle is rigid, it cannot appropriately relax during diastole, resulting in this condition. As a result, Heart failure with preserved ejection fraction (HFpEF) occurs. Acute or chronic cardiac failure is still another possibility. Acute breathing issues caused by decompensated heart failure might exacerbate the symptoms of chronic heart failure. Chronic heart failure is a long-term illness treated by treating the symptoms. Increased cardiac demand can increase left ventricular diastolic pressure, which can lead to high-output heart failure and pulmonary congestion. Other illnesses can induce heart failure, yet they should not be mistaken with heart failure. Cardiac arrest or asystole is the medical term for when the heart stops beating. They have the potential to cause premature mortality if ignored. Myocardial infarction (often referred to as a "heart attack") happens when the heart's blood supply is cut off. Cardiomyopathy specifically refers to defects in the heart muscle, leading to heart failure. Ischemic cardiomyopathy causes myocardial infarction, which proves that coronary artery disease is to blame for the condition in question. Dilated cardiomyopathy is a sign that the heart muscle has dilated due to its damage. However, hypertrophic cardiomyopathy is characterized by the expansion and thickness of the heart muscle [19-23].

1.3   Heart Failure with Myocardial Infarction

Heart failure (HF) is most often caused by an acute myocardial infarction (AMI), despite significant progress made in the treatment of coronary artery disease (CAD) and AMI in the last two decades [24]. To distinguish between cases where heart failure develops before, during, or after a MI hospitalization, it is necessary to look at the time sequence in which the heart failure first occurs. AMI triggers metabolic imbalance and myocyte death. Myocyte enlargement and interstitial fibrosis are two mechanisms by which the heart reacts to cell loss. An increased ventricular volume and a rightward shift in EDPVR are two structural alterations that occur over time in the LV. The LV becomes more spherical due to these structural changes [25]. "Ventricular remodeling" refers to these morphological, biochemical, and molecular alterations.

AMI can cause premature morbidity and death. The risk of HF persists despite improvements in early survival following ST-segment elevation MI (STEMI). In particular, LV systolic function, LV ejection fraction (LVEF), is the standard of treatment for determining the first severity of heart damage. A computational approach to ventricular biomechanics can reveal insights into the heart's function and dysfunction when coupled with clinical imaging. Computational heart models have been developed from simple representations to more realistic image-derived cardiac models [26].

1.3.1 Myocardial infarction-related heart failure occurred during hospitalization

Myocardial infarction, myocardial shock, and mechanical complications, such as heart muscle rupture, ventricular septal defect, and ventricular free wall rupture, all contribute to the development of HF at the time of the MI hospitalization. In the first 30 minutes of ischemia, cardiomyocyte structure alterations and swelling emerge, resulting in more myocyte death after 3 hours of ischemia. Thrombus embolism continues to cause microvascular dysfunction and myocardial ischemia despite effective epicardial reperfusion. The inflammatory reaction to the death of myocytes also plays a role in the development of HF. There have been two distinct trends in heart failure (HF) incidence during the past few decades. Although death rates have decreased since recent advancements in pre-hospital treatment, there has been a rise in HF at MI presentation. Percutaneous coronary intervention (PCI) may have contributed to the decrease in in-hospital HF since PCI has been shown to result in more myocardial salvage than

thrombolysis. From 1996 to 2008, in-hospital HF aggravating MI incidence has decreased from 46% to 28% in the SWEDEHEART registry [24]. If troponin levels are used to determine the severity of an MI, it may be possible to identify patients at a lesser risk for heart failure. Patients with larger infarcts, and those who have late or failed epicardial or microvascular bed reperfusion have more significant LV remodeling. About 13% of patients are diagnosed within 30 days and 20–30% within a year of being discharged from the hospital for MI. There is a significant incidence of HF in the first few months following release from the hospital; however, the rate steadily decreases and remains steady at 1.3–2.2% every year [24].

1.3.2 Heart failure's clinical consequences following myocardial infarction

Regardless of the type of HF, the development of HF following MI has a major influence on outcomes. Those with a history of MI are three times more likely to die overall and four times more likely to die from cardiovascular disease if they develop heart failure. Adverse effects are also influenced by the time of HF development. Patients who acquire HF more than three days after a heart attack have a 43% greater mortality risk than those who develop HF during the first three days [24]. This may be due to distinct risk factors and processes that contribute to HF at different stages in time.

1.3.3 Screening and prevention of heart failure

The European Society of Cardiology and the American Heart Association has made it clear that HF prevention is a significant public health issue. In the post-MI population, screening and prevention of HF are of special relevance because of the elevated risk of developing HF. A missed or delayed diagnosis negatively impacts HF patients' prognosis and treatment expenditures. Patients at high risk for developing HF should be closely monitored, which has been found to improve patient adherence and increase prescribed medication; fewer cardiovascular hospitalizations should be expected as a consequence [24].

1.3.4 Progression of Heart Failure and MI

When a major coronary artery is completely blocked, an MI occurs. Cell death advances from the sub-endocardium to the sub-epicardium in a time-dependent manner within the perfusion area of the blocked artery. Flow deprivation is most severe in the sub-endocardium. Studies have argued that dogs have a well-developed system of epicardial coronary collaterals,

making the sub-endocardium the most susceptible myocardial area in this species. It's important to remember that the LV wall has transmural heterogeneity, as evidenced by differences in myocardial blood flow and metabolism, contraction and relaxation dynamics, and myocardial pressure and strain. According to the literature review, there is no anatomic justification for a lateral expansion of the border danger zone [27].

The magnitude of an infarct is related to mortality and the development of HF. The adaptive cardiomyocyte hypertrophy increases in proportion to the size of the infarct and the remaining viable myocardium. Following an MI, the ventricular remodeling process begins as outlined in the preceding paragraphs. As a result, clinical studies aiming at preventing HF following an AMI focus primarily on reducing myocardial damage. There have been two main approaches taken. The first step is to reduce the time the heart is in a state of ischemia. Put another way, "time is muscle" says that infarct size decreases as quickly as the artery can be reperfused and the myocardial oxygen supply is restored. Reducing reperfusion damage is the second way to keep the size of an AMI infarct to a minimum. However, none of these techniques has been successful in ordinary clinical practice despite considerable evaluation and excellent preclinical data. To yet, clinical trials have not been investigated to lower myocardial oxygen demand to establish a more favorable supply-demand ratio as a means of minimizing infarct size, even though early reperfusion treatment is the current paradigm. Preclinical and clinical research suggests that lowering the heart's mechanical workload (unloading) before reperfusion decreases infarct size. Ongoing preclinical studies have shown that unloading can reduce the extent of an infarct and prevent the onset of heart failure (HF). This method can be successfully applied in the clinic [25].

AMI patients need rapid pain management, life support, and myocardial damage restriction to keep the infarct size under control and avoid re-infarction. Risk assessment should also be performed on any patient who has had an AMI or has asymptomatic left ventricular dysfunction or heart failure. AMI patients are joining a system of acute and chronic illness treatment that includes both "medical" as well as "interventional" components when they are hospitalized [27].

1.4 Left ventricular thrombus

A left ventricular thrombus (LVT) is a blood clot that forms in the heart's LV. LVT is a frequently occurring consequence of AMI. Typically, the clot is a mural thrombus located on

the ventricle's wall. The greatest danger associated with LVT is the development of cardiac embolism, a condition in which the thrombus detaches from the ventricular wall and travels through the circulation, obstructing blood vessels. The blockage is particularly detrimental to the heart and brain (stroke). According to the American Heart Association, AMI thrombus is a relatively uncommon complication, with an incidence of between 2.9% and 15% in different populations. Patients' prognosis and quality of life with a thrombus in the LV may be worse. Frontal ST-elevation MI (STEMI), large infarct size, LV aneurysm, suboptimal revascularization (those with TIMI), and cardiac arrest are all risk factors [29].

1.4.1 Thrombus formation in the LV

Virchow-triad is the primary mechanism of thrombosis formation [30]. There are three factors involved in Virchow-triad (Figure 1.12) formation of LVT after AMI: hypercoagulability, endothelial injury, and blood stasis. In the event of tissue necrosis, LV dyskinesis or akinesis occurs, resulting in blood stasis in the intracavitary region.
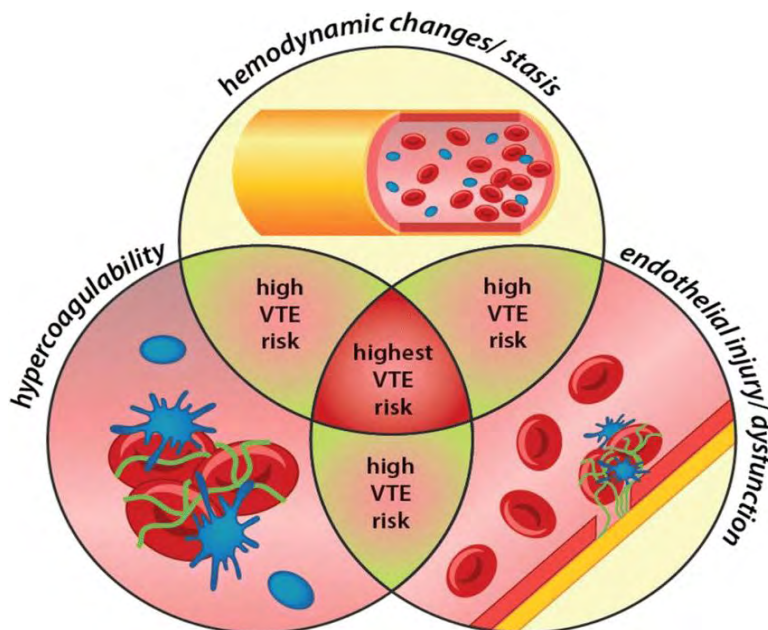
Figure 1. 8: Virchow's triad: hemodynamic changes, endothelial injury, and hypercoagulability are risk factors for venous thrombosis. VTE: venous thromboembolism, is the medical term for this condition [30].

Other pathological states, such as stress cardiomyopathy, have rates of LVT that are as low as 1 - 2% in the hospital, even though anticoagulation is rarely used (4 - 8% of patients) [29]. As a result, both the inciting event and myocardial substrate may influence the risk of

LVT formation beyond LV dysfunction. Inflammation and collagen exposure in sub-endothelial tissue serves as necrotic tissue for platelet aggregation and activation of the clotting cascade. Following a MI, hypercoagulable states can persist for up to six months. Obsession, platelets, and red blood cells infarct in the left ventricle (LV) [30].

1.5   Finite Element Analysis of Human Heart

Predictive medicine applications in cardiovascular surgery can be improved by using a high-quality geometric model of the human heart to simulate the circulatory system. An essential part of the simulation is the use of finite element analysis. The heart model requires adaptive and high-quality tetrahedral finite element meshes. For the cardiac model, the tetrahedral mesh creation has three key issues: First, the model is acquired by modifying the model and creating volumetric gridded data. Secondly, extraction of quality tetrahedral mesh from volumetric gridded data that is adaptive and flexible, and finally, detection of material and boundary layers.

Cardiovascular disease can be better understood by using computational modelling of the heart, which combines imaging science with mathematics, informatics, and cardiovascular biology. Using high-resolution medical imaging, computer models of blood vessels and the heart can now be created more authentic than ever before. When it comes to solving the 3D model of the heart, an effective FEM solver is applied [31]. As a result, cardiovascular informatics has become a more advanced field. 3D computer models of the heart's structure and function and clinical data may be used to generate a patient-specific model of cardiovascular illness. Computational simulations may be utilized to develop cardiovascular system components' mechanical and biological aspects at a low cost. After the heart's architecture and structure have been constructed in 3D, an electrical model of the myocardium may be generated. As well as the overall organ function, electromechanical heart models may also replicate the molecular structure of the organ [32]. Pathological changes may influence electromechanical performance by altering the heart's structure and function [33]. There are independent studies of cardiac and vascular hemodynamics. More complicated mathematical lumped-parameter models are combined in advanced computational modelling to represent the heart's cycle better. Boundary conditions significantly influence the validity of computational hemodynamic models; hence, their accuracy is crucial.

Computational modelling is widely regarded as a cost-effective and reliable method of optimizing device design by manufacturers and regulators. Computational models might be used to design virtual intervention/surgery in complex clinical situations by adjusting the kind of device, size, and procedural parameters [33]. Computational models of the heart face various challenges before they can be employed in clinical practice. There has been tremendous growth in recent years in the use of FEM techniques to model various cardiac compartments in order to correctly reproduce human physiology. Cardiovascular research has just recently begun to investigate models of heart failure pathophysiology that may mimic the physiological, hemodynamic and functional aspects of myocardial infarction [33].

1.6 Background and present state of the problem

Nearly 70% of HF cases are caused by adverse remodeling of the LV (LV) after AMI. Premature morbidity and death are typical outcomes of AMI. At the time of the MI hospitalization, factors contributing to the pathogenesis of HF development include myocardial compromise caused by necrosis, myocardial stunning, and mechanical complications such as papillary muscle rupture, ventricular septal defect, and ventricular free wall rupture. Within 30 minutes of ischemia, structural changes and oedema in cardiomyocytes develop, progressing to myocyte death after 3 hours. Through the production of reactive oxygen species, reperfusion itself causes a second wave of injury. Whether epicardial reperfusion is successful, embolization of thrombotic debris results in persistent microvascular dysfunction and myocardial ischemia [24].

Additionally, the inflammatory response to myocyte death plays a role in developing HF. Long-term HF risk remains consistently high, despite improvements in early survival after STEMI. LV systolic function, and in particular the LV ejection fraction, are the gold standards for determining the early severity of a heart injury. It is important to keep in mind that global measurements of LV pump performance, such as myocardial contractility and stiffness, are oversimplified. There are various factors for which the blockages in the coronary arteries may appear such as the plaque formation, deposition of cholesterol, fat, calcium etc. in the lining of coronary arteries. After a certain limit of these depositions, the coronary arteries become narrow and stiff. Consequently, the blood flow is restricted and the heart is required to develop high blood pressure to pump the blood throughout the body. Subsequently the myocytes (heart muscle cells) suffer from the lack of sufficient oxygen and proteins. These result the deaths of

the myocytes and cut off the blood flows through the affected arteries. Clinically it is difficult to diagnose the AMI HF due to having very limited robust therapies, expensive treatment, long-term clinical assessment, complexities in in-vivo measurements etc.

Computational ventricular biomechanics combined with clinical imaging is becoming more popular as a tool for studying heart function and dysfunction. The heart's capacity to effectively pump blood into the body is largely dependent on myocardial contractility. As soon as an infarction occurs, doctors must assess how much damage has occurred to the myocardium. When determining which tissues are alive and which are not, cardiologists would benefit from having a noninvasive technique for assessing regional cardiac contractility. For the treatment of infarct-induced heart failure, this instrument may also assess the effectiveness of surgical treatments and medicinal equipment. To assist surgeons in deciding where to incise and how much of the LV infarct area to spare, the most significant benefit would be provided [34]. From the literature review, it is seen that the FEM modeling of LV with MI has been used to investigate the effects of infarction zones on the performance of systemic blood circulation through the coronary arteries of the heart [36-39]. However, the FEM frameworks of LV with MI have not been well established yet. Very limited research was performed to investigate the effects of infarct zone sizes and locations of the infarct zones on the overall function of the LV. No direct correlations among the infarct size, location, contractility, and tissue stiffness with respect to LV function have been found in the existing research. In this research, we have emphasized to investigate the effects of infarct size and infarct location on the function of LV. In addition, we have explored the effect of increased tissue stiffness and decreased contractility on the LV function for MI cases. Therefore, the current model of LV with MI would help us to assess the effects of infarct zone, infarct location, decreased contractility, and increased tissue stiffness on the function of the LV.

1.7   Objectives of the Study

When simulating the cardiac cycle with MI, we'll use a closed-loop lumped parameter circulatory model in conjunction with a LV finite element model with realistic geometry and microstructures. The baseline model will be calibrated using data from the available clinical studies of MI patients.

The particular goals of this study are:

1. To calibrate the model of left ventricular finite element model to simulate MI patient by using the existing clinical measurements.

2. The calibrated model of LV MI patients will be utilized to quantify the contributions of the infarct size, infarct location, stiffness and contractility of the infarcted tissue on the LV hemodynamic and functional indices, such as PV loop, circumferential, longitudinal and radial strains.

CHAPTER 2
LITERATURE REVIEW

The main cause of death in the world is heart disease. Computer models simplify identifying the differences between a healthy and a diseased heart's mechanics. In recent decades, the realistic geometry and architectural structure of cardiac muscle fibers in FE models have advanced substantially. It is possible to integrate electrophysiology and mechanics and achieve long-term remodeling of the heart using these models. There has been an increase in using computer models instead of animal and clinical studies to characterize heart disease pathophysiology and treatment procedures, such as cardiac resynchronization therapy and ventricular surgical restoration [38]. Computational models can be used to supplement animal and clinical research because of their vast diversity and inexpensive cost. In the animal study, just a few variables may be altered without affecting the others. Heart disease pathophysiology can be difficult to distinguish since so many variables might have an influence on it. Individual parameters can be studied without having to take into account the confounding effects of other factors when using computer models that are verified using physiological principles [40-41]. Still, there are a lot of issues that need to be resolved or improved. Realistic cardiac models will allow the researchers to address critical questions about human heart disease that cannot be solved through trials. In the case of an emergency, a patient-specific medical plan may be quickly developed using models like this one, whereas the standard treatment approach takes much longer.

According to the available literature, either an electrical circulatory system analogue or a separate FE heart model was built and used with the FE model in either an open [40-42] or closed-loop [38]. The coupled electrical analogue was constructed using a simplified description of the peripheral cardiac system based on a time-varying elastance function. Pulsatile models [33] and outlet boundary restrictions are often employed in open-loop circulatory modelling frameworks to mimic blood ejection. The process's outputs are constrained by physiological considerations. By increasing and contracting the ventricular cavity capacity, isovolumic phases and expansion may be simulated. A closed pressure-volume loop may be created by optimizing the modelling framework's free parameters using any of these two ways. A closed-loop circulatory modelling framework looks more physical since the complete amount of blood in the cardiovascular system is naturally conserved. The ventricular-arterial interactions and the peripheral cardiovascular system are simulated using a highly

idealized electrical circuit, such as a resistor, capacitor, and voltage generator. It has been a major challenge in developing cardiovascular system mathematical models since the very beginning. In the early stages of this idea, mechanical elements in the surrounding environment were used to stimulate the heart muscle to contract. However, this is an inaccurate depiction of how the heart works. If model predictions are based on well-established physiological principles, proper representation of ventricular active contraction activity is essential. The intricate process of active contraction involves various factors, including calcium ion association-dissociation, the number of actin sites available for myosin response, classical kinetics, differential equations, and more. As for active fiber stress in cardiac muscle, several other constitutive relationships [46] have been proposed. It is possible to match experimental data from the literature using a variety of factors. The meaning of "active contraction" is always being revised, and research into this topic is ongoing.

MI is a leading cause of premature death and morbidity in the world. Long-term heart failure risk is continuously high, despite improvements in early survival following ST-segment elevation MI (STEMI). LV systolic function, and in particular, LV ejection fraction (LVEF), is the standard of treatment for determining the first severity of heart damage [26]. However, global assessments of LV pump performance are unsophisticated compared to biomechanical characteristics such as myocardial contractility and stiffness.

Systolic performance (systolic shortening and wall thickening) following anteroapical myocardial infarction (MI) is reduced in the non-ischemic border zone (BZ). The infarct was previously assumed to be the cause of the impaired BZ function. It has been shown that the BZ contractility is lowered by more than 50% in FE-based inverse computations of regional contractility, in which optimization processes aim to match calculated and empirically recorded left ventricular (LV) volume and strain. After anteroapical MI, the BZ contractility appears to change linearly across the BZ, and the BZ may be as wide as 3 cm in diameter.

Posterolateral or inferior LV wall myocardial infarction (MI) is distinct from anteroapical LV wall myocardial infarction (MI). Preventing posterolateral MI from expanding and improving survival rates are the main benefits of this kind of MI. Posterolateral MI causes the posterior papillary muscle to migrate laterally, which causes persistent ischemic mitral regurgitation [41]. Because of this, it is probable that the reduction in BZ contractility following

posterolateral MI is distinct from that following anteroapical MI, and that LV remodeling and the development of ischemic mitral regurgitation may be impacted by this difference.

One of the difficulties in modeling the heart is that the constitutive myocardial parameters need to be established first. To estimate these parameters, a variety of methods have been established by comparing the available clinical measures (displacement, strain, or pressure-volume curve). It has been shown that an image-based model of the LV may be utilized to restore stresses to a normal level by matching strain and volume data to create a reference stress map. The integration of active myocardial contraction in the prediction of systolic stress in the LV wall is necessary. Despite this, the biomechanics that contributes to LV unfavorable remodeling and heart failure remains a mystery [26]. In recent years, the modelling of sick hearts has received much attention. Using a Fung-type constitutive law, Guccione and colleagues [26] observed that myofiber stress is raised in the infarct zone, and contractility in the border zone is reduced. They have also suggested that the post-MI remodeling may be negatively impacted by the altered mechanical environment [26]. Myocardial contractility in the distant areas of the MI rose ten days after acute-MI, followed by a further rise 38 days later, according to a biomechanical pig heart model developed by Chabiniok et al. [26] Using patient-specific clinical data, Gao et al. [26] found that the amount of contractility required by the myocardium after an acute MI was much more than in a control heart, suggesting an enhanced usage of the contractile reserve in the distant myocardial zone for the patient. For the second time, ironically, patients with dilated cardiomyopathy had higher peak contractility than healthy volunteers when Asner et al. [26] used individualized mechanical LV models to assess peak contractility. Nevertheless, when cardiac contractility was evaluated using computer models, the differences between healthy and sick hearts were substantial. Inter-individual differences, sample size, or technical variables may be blamed for this discrepancy.

Sacks and Humphrey et al. [42] have published passive ventricular tissue biaxial mechanical testing findings for material qualities and mechanical analysis. Hunter and McCulloch's group published several key articles regarding how the structure of the ventricle's fibers affects its mechanical conditions [42]. Ultrasound elastic tensor imaging is equivalent to magnetic resonance diffusion tensor imaging in terms of fiber orientation. Sommer et al. [42] show that the passive human heart may be regarded as a nonlinear, anisotropic, viscoelastic, history-dependent soft biological material through biaxial extension and triaxial shear. Yap et

al. [42] used a biaxial tester and 3D ultrasound speckle tracking to examine the myocardium of rats. Using shear wave imaging, Lee et al. [42] attempted to measure the orientation of fibers in an open chest animal model. Shear wave imaging was used by Couade et al. [42] to evaluate changes in myocardial stiffness during the cardiac cycle. According to Holmes et al. [42], big collagen fiber structure is a key factor in determining the mechanical characteristics of scars. More recently, Holmes et al. [42] found that image-based cardiac mechanical models might be effective for clinical and surgical applications. The passive mechanical characteristics of a porcine infarct were determined by Mojsejenko et al. [42] using MRI and finite element techniques. McGarvey et al. [42] used in vivo MRI and finite element simulations to study changes in infarct material characteristics over time. Using cine and tagged MRI scans and LV cavity pressure recordings, Xi et al. developed a technique for calculating the diastolic mechanical characteristics of the left ventricle (LV) by distinguishing passive myocardial constitutive properties from diastolic residual active tension [42]. Peskin's famous first model with moving boundaries using immersed-boundary method [42], the early MRI-based models for mechanical analysis and investigations by Axel and Saber and McCulloch's [42] passive/active models, including the Continuity package, have all been developed to investigate cardiac mechanics with potential clinical applications. The authors have developed patient-specific CMR-based RV/LV models with fluid-structure interactions (FSI) that may be used for various surgical designs and prospective applications. It has been shown that patients with MI have different morphology, mechanics, and biology than healthy volunteers.

Under four scenarios, Sack et al. [42] describe major recent advancements in the Living Heart Model (LHM) and utilize the LHM to compute left ventricular (LV) and right ventricular (RV) myofiber stress distributions. Acute left heart failure (ALHF) treated with an LV assist device flow rate of 2 L/min. ALHF treated with an LV assist device flow rate of 4.5 L/min for ALHF. Four sheep with LV infarcts and six sheep with infarcts repaired surgically were studied by Walker and colleagues. They used cardiac catheterization, three-dimensional MRI with tissue tagging, MR diffusion tensor imaging, and an advanced FE method (explicitly developed for cardiac mechanics to measure regional systolic myocardial material properties in the beating hearts of these animals. But even though both prior types of research represent major breakthroughs, they both used a manually led pseudo-optimization. On the other hand, Sun et al. and Wenk et al. [35] employed mathematical models of infarcted LV to define and quantify its regional contractility. On the other hand, these models assume that the contractility in the

BZ, distant, and infarct areas is homogenous. This results in a sudden shift in contractility at infarction–BZ and remote borders.

We used finite element modelling (FEM) to explore the impact of myocardial infarction on the function of the left ventricle (LV). It has become more common for people with heart disease to suffer from a severe MI. The underlying cause of acute MI remains a mystery due to a lack of adequate clinical studies and research resources. To the best of our knowledge, very few studies using finite element modeling have been conducted on the MI in the past. In our study, we have focused on finding out the effects of infarct size and location by changing the contractility and other relevant model parameters, which directly influence the overall function of the LV.

CHAPTER 3

MODELING THE LEFT VENTRICLE AND CIRCULATORY SYSTEM

This chapter discusses a left ventricle finite element model and a systemic circulation model.

3.1 Modelling the Systemic Circulatory System

A closed-loop lumped parameter circulatory model was used for the systemic circulatory system which was coupled to the LV finite element model.
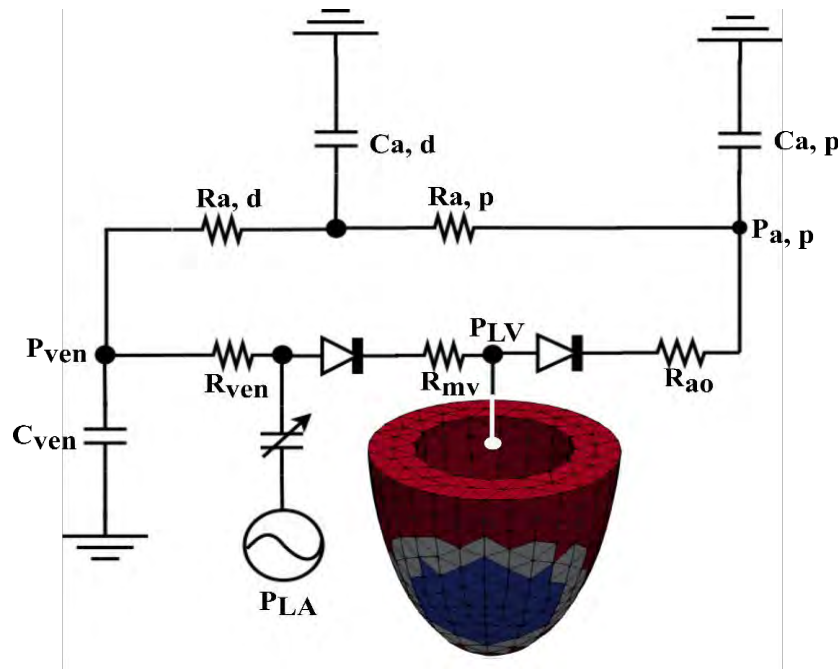
Figure 3. 1: Schematic diagram of the modeling framework showing the LV FE model and other compartments of the systemic circulation which were modeled using their electrical analog [46].

To connect finite element models of the LV, a closed-loop modeling technique for the systemic circulation circuit was used. The other circuit components were modeled using electrical analogs (Figure 3.1). Since the entire mass of blood in the circulatory system has to be preserved, the rate of volume change in each storage compartment of the circulatory system must be coupled to the net change in inflow and outflow rates by the following equations (Eq. 1-4) [46].

$$\frac{dV_{LV}(t)}{dt} = q_{mv}(t) - q_{ao}(t) \tag{1}$$

$$\frac{dV_{a,d}(t)}{dt} = q_{a,p}(t) - q_{a,d}(t) \tag{2}$$

$$\frac{dV_{LA}(t)}{dt} = q_{ven}(t) - q_{mv}(t) \tag{3}$$

$$\frac{dV_{ven}(t)}{dt} = q_{a,d}(t) - q_{ven}(t) \tag{4}$$

$$\frac{dV_{a,p}(t)}{dt} = q_{ao}(t) - q_{a,p}(t) \tag{5}$$

Where, q_{mv}, $q_{a,p}$, q_{ao}, q_{ven}, and $q_{a,d}$ are volumetric flow rates at various segments, whereas V_{LV}, $V_{a,d}$, V_{LA}, V_{ven}, and $V_{a,p}$ are volumes of the LV, distal artery, LA, vein, and proximal artery, respectively. The flow resistances of the respective components (R_{ven}, $R_{a,p}$, $R_{a,d}$, R_{ao}, and R_{mv}) and the pressure drop between neighboring compartments determine the volumetric flowrates of distinct components of the circuit. The flow rates are calculated based on the following equations (Eq. 6-10) [46].

$$q_{ven}(t) = \frac{P_{ven}(t) - P_{LA}(t)}{R_{ven}} \tag{6}$$

$$q_{a,p}(t) = \frac{P_{a,p}(t) - P_{a,d}(t)}{R_{a,p}} \tag{7}$$

$$q_{mv}(t) = \begin{cases} \frac{P_{LA}(t) - P_{LV}(t)}{R_{mv}} & \text{when, } P_{LA}(t) \geq P_{LV}(t) \\ 0 & \text{when, } P_{LA}(t) < P_{LV}(t) \end{cases} \tag{8}$$

$$q_{ao}(t) = \begin{cases} \frac{P_{LV}(t) - P_{a,p}(t)}{R_{ao}} & \text{when, } P_{LV}(t) \geq P_{ap}(t) \\ 0 & \text{when, } P_{LV}(t) < P_{a,p}(t) \end{cases} \tag{9}$$

$$q_{a,d}(t) = \frac{P_{a,d}(t) - P_{ven}(t)}{R_{a,d}} \tag{10}$$

The volume of each component determines the pressure drop. The simplified pressure and volume relationships were established for the veins, proximal, and distal arteries, as shown below (Eq. 11-13) [46].

$$P_{ven}(t) = \frac{V_{ven}(t) - V_{ven,0}}{C_{ven}} \tag{11}$$

$$P_{a,p}(t) = \frac{V_{a,p}(t) - V_{ap,0}}{C_{a,p}} \tag{12}$$

$$P_{a,d}(t) = \frac{V_{a,d}(t) - V_{ad,0}}{C_{a,d}} \tag{13}$$

The constant volumes at the rest of the veins, proximal, and distal arteries are $V_{ven, 0}$, $V_{ap, 0}$, and $V_{ad, 0}$, respectively. The total passive stiffness of the veins, proximal, and distal arteries is represented by C_{ven}, $C_{a, p}$, and $C_{a, d}$, respectively. However, the following equations (Eq. 14-17) [46], which use a time-varying elastance function to describe the contraction of the left atrial, required that pressure in the left atrium $P_{LA}(t)$ be a function of its volume $V_{LA}(t)$.

$$P_{LA}(t) = e(t)P_{es,LA}(V_{LA}(t)) + (1 - e(t))P_{ed,LA}(V_{LA}(t)) \tag{14}$$

where,

$$P_{es,LA}(V_{LA}(t)) = E_{es,LA}(V_{LA}(t) - V_{0,LA}) \tag{15}$$

$$P_{ed,LA}(V_{LA}(t)) = A_{LA}(e^{B_{LA}(V_{LA}(t) - V_{0,LA})} - 1) \tag{16}$$

And,

$$e(t) = \begin{cases} \frac{1}{2}\left(\sin\left[\left(\frac{\pi}{t_{\max}}\right)t - \frac{\pi}{2}\right] + 1\right); & 0 < t \leq 3/2 t_{\max} \\ \frac{1}{2}e^{-(t - 3/2 t_{\max})/\tau_{LA}}; & t > 3/2 t_{\max} \end{cases} \tag{17}$$

In Eq. (15-16), $V_{0, LA}$ is the volume axis intercept of the end-systolic pressure-volume relationship (ESPVR), A_{LA} and B_{LA} are parameters of the left atrium's end-diastolic pressure-volume relationship (EDPVR), and $E_{es, LA}$ is the end-systolic elastance. The Eq. (17) gives the driving function $e(t)$, where τ is the relaxation time constant and t_{max} is the maximum chamber elastance point. Table 3.1 shows the values of $E_{es, LA}$, $V_{0, LA}$, A_{LA}, B_{LA}, t_{max}, and τ_{LA}.

Table 3. 1: Time varying elastance model parameters for left atrium [46].

Parameters	Units	Values (Normal and AMI heart LV baseline)
End-systolic elastance, $E_{es,LA}$	Pa/ml	60
Scaling factor for EDPVR, A_{LA}	Pa	58.67
Time constant of relaxation, τ	ms	25
Exponent for EDPVR, B_{LA}	ml^{-1}	0.05
Time to end-systole, t_{max}	ms	120
Volume axis intercept, $V_{0,LA}$	ml	10

Furthermore, the LV pressure is a function of its corresponding volume that can be correlated by a non-closed form function as shown in the following equation [46],

$$P_{LV}(t) = f^{LV}(V_{LV}(t)) \qquad (18)$$

The functional relationship between LV pressure and volume was determined using the FE approach, as explained below. The parameter values for the closed-loop circulatory model are listed in Table 3.2.

Table 3. 2: Fixed values of the model parameters for all simulation cases.

Parameter	Unit	Values
Aortic valve resistance, R_{ao}	Pa ms ml^{-1}	500
Proximal aorta resistance, $R_{a,p}$	Pa ms ml^{-1}	18000
Venous resistance, R_{ven}	Pa ms ml^{-1}	100
Mitral valve resistance, R_{mv}	Pa ms ml^{-1}	200
Proximal aorta compliance, $C_{a,p}$	ml Pa	0.0032
Distal aorta compliance, $C_{a,d}$	ml Pa	0.033
Venous compliance, C_{ven}	ml Pa	0.28
Resting volume for proximal aorta, $V_{ap,0}$	ml	360
Resting volume for distal aorta, $V_{ad,0}$	ml	40

3.2   Formulation of The Left Ventricular Finite Element model

For the LV finite element formulation, the weak form was obtained via minimizing of these Lagrangian functionals [46]:

$$\mathcal{L}(\boldsymbol{u}, p, P_{cav}, \boldsymbol{c}_1, \boldsymbol{c}_2) \qquad (19)$$
$$= \int_{\Omega_0} W(\boldsymbol{u})dV - \int_{\Omega_0} p(J-1)dV - P_{cav}(V_{cav}(\boldsymbol{u}) - V) - \boldsymbol{c}_1 \cdot \int_{\Omega_0}$$
$$\boldsymbol{u}dV - \boldsymbol{c}_2 \cdot \int_{\Omega_0} \boldsymbol{X} \times \boldsymbol{u}dV$$

P_{cav} is the Lagrange multiplier used to limit the LV cavity volume $V_{cav}(u)$ to a certain value of V [46] when u is the displacement field, p multiplier enforces tissue incompressibility (i.e., Jacobian of the deformation gradient tensor J = 1), and both c_1 and c_2 are Lagrange multipliers

that limit rigid body translation (i.e. zero mean translation) and rotation (i.e., zero mean rotation) [46]. Cavity volume V_{cav} in the left ventricle is determined by

$$V_{\text{cav}}(\boldsymbol{u}) = \int_{\Omega_{\text{inner}}} dv = -\frac{1}{3}\int_{\Gamma_{\text{inne}}} \boldsymbol{x}.\boldsymbol{n}da \tag{20}$$

Where, Γ_{inner} is the inner surface, n is the normal unit vector, and Ω_{inner} is the enclosed volume by the inner and basal surface at $z = 0$.

The solution produced by minimizing the functional specified pressure-volume relationship of the left ventricular (LV) is necessary for the lumped parameter circulatory model [46]. Using Eq. (19)'s first functional variant, we get the following equation.

$$\delta\mathcal{L}(\boldsymbol{u}, p, P_{\text{cav}}, \boldsymbol{c}_1, \boldsymbol{c}_2) = \int_{\Omega_0} (\boldsymbol{P} - p\boldsymbol{F}^{-T}) \tag{21}$$
$$: \nabla\delta\boldsymbol{u}dV - \int_{\Omega_0} \delta p(J-1)dV - P_{\text{cav}}\int_{\Omega_0} \text{cof}(\boldsymbol{F})$$
$$: \nabla\delta\boldsymbol{u}dV - \delta P_{\text{cav}}(V_{\text{cav}}(\boldsymbol{u}) - V) - \delta\boldsymbol{c}_1 \cdot \int_{\Omega_0} \boldsymbol{u}dV - \delta\boldsymbol{c}_2 \cdot \int_{\Omega_0} \boldsymbol{X}$$
$$\times \boldsymbol{u}dV - \boldsymbol{c}_1 \cdot \int_{\Omega_0} \delta\boldsymbol{u}dV - \boldsymbol{c}_2 \cdot \int_{\Omega_0} \boldsymbol{X} \times \delta\boldsymbol{u}dV$$

Where, F and P are the deformation gradient and first Piola Kirchhoff stress tensor, respectively. δP_{cav}, δc_1, δc_2, δu, and δp are the volume constraint, zero mean translation and rotation, variation of the displacement field, and Lagrange multipliers for enforcing incompressibility, respectively. The next step in the Euler-Lagrange equations is to discover $u \in H^1 (\Omega_0)$, $p \in L^2 (\Omega_0)$, $P_{cav} \in \mathbb{R}$, $c_1 \in \mathbb{R}^3$, $c_2 \in \mathbb{R}^3$ that satisfies Eq. (22).

$$\delta\mathcal{L}(\boldsymbol{u}, p, P_{\text{cav}}, \boldsymbol{c}_1, \boldsymbol{c}_2) = 0 \tag{22}$$

And, $u_z|_{base} = 0$ (the deformation basal constraints to restrict in-plane) $\forall\delta u(\Omega_0)$, $\delta p \in L^2 (\Omega_0)$, $\delta P_{cav} \in \mathbb{R}$, $\delta c_1 \in \mathbb{R}^3$, $\delta c_2 \in \mathbb{R}^3$.

3.3 The LV's constitutive law

The mechanical behavior of LV has been described by using the formulation of active stress in the systemic circulation. As a result of this formulation, the stress tensor P may be divided into two parts: a passive one, P_p, and an active one, P_a. In order to calculate the passive

stress tensor, we used the formula $P_p = dW/dF$, where W is the strain energy function [46], given by,

$$W = \frac{1}{2} C(e^Q - 1) \tag{23}$$

Where,

$$Q = b_{ff}E_{ff}^2 + b_{xx}(E_{ss}^2 + E_{nn}^2 + E_{sn}^2 + E_{ns}^2) \tag{24}$$
$$+ b_{fx}(E_{fn}^2 + E_{nf}^2 + E_{fs}^2 + E_{sf}^2)$$

C is a material property (unit is Pa) that may be changed to vary the material's stiffness (similar to Young's modulus). To provide polar anisotropic response, the values of material parameters b_{ff}, b_{xx}, and b_{fx} may be changed to modify the stiffness along the direction of myofibers and the plane perpendicular to the myofibers. The values of the material parameters b_{ff}, b_{xx}, and b_{fx} employed in this model are taken from earlier research [46]. The parameter C has been changed to match the normal and HFpEF patients' measured end-diastolic pressure (EDP). E_{ij} is a component of the Green-Lagrange strain tensor E_{LV} in Equation (24), with *(i j)* $\in$ *(f, s, n)* designating the myocardial fiber, sheet, and sheet normal directions, respectively (Figure 3.2).
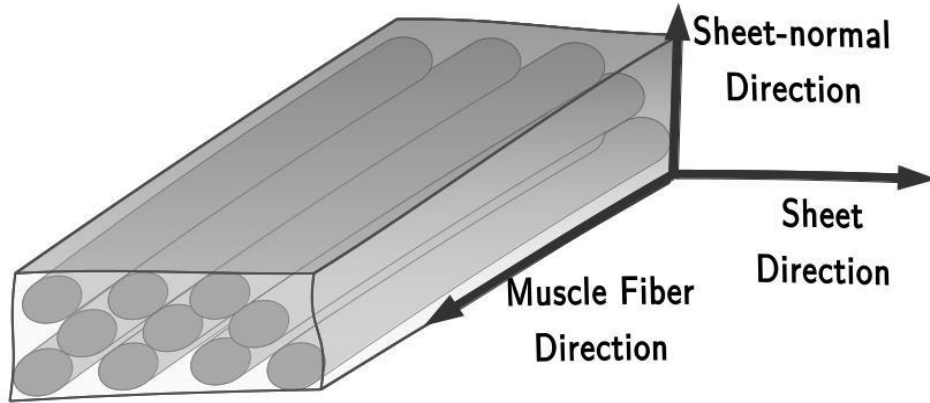
Figure 3. 2: Myocardial fiber direction f, sheet direction s and sheet normal direction n [47].

A modified time-varying elastance model is used to find the active stress P_a along the direction of the local fiber [46].

$$\boldsymbol{P}_{\text{LV,a}} = T_{ref} \frac{Ca_0^2}{Ca_0^2 + ECa_{50}^2} C_t \mathbf{e}_f \otimes \mathbf{e}_{f_0} \tag{25}$$

This equation has four variables: e_f, e_{fo}, T_{ref}, and Ca_0, which stand for the local vectors describing muscle fiber direction in their present and reference configurations, respectively.

The calcium sensitivity ECa_{50}, which varies with length, and the constant C_t are given by Equations (26-27) [46].

$$ECa_{50} = \frac{(Ca_0)_{max}}{\sqrt{\exp\big(B(l - l_0)\big) - 1}} \tag{26}$$

$$C(t) = \begin{cases} \frac{1}{2}\left(1 - \cos\left(\pi\frac{t}{t_0}\right)\right) & t < t_t \\ \frac{1}{2}\left(1 - \cos\left(\pi\frac{t_t}{t_0}\right)\right)\exp\left(\frac{t - t_t}{\tau}\right) & t \geq t_t \end{cases} \tag{27}$$

As shown in Eq. (26), B is a constant, and $(Ca_0)_{max}$ is the highest intracellular calcium concentration, and l_0 is the length of sarcomere at which no active tension arises. As shown in Eq. (27), peak tension is reached in t_0, isovolumic LV relaxation begins in t_t, and isovolumic relaxation has a time constant of τ. Tabulated in Table 3.3 are the LV model parameter values.

Table 3. 3: Fixed parameter values of the LV FE model.

Parameter	Unit	Values
Exponent of strain energy function, b_{ff}	Unitless	29
Exponent of strain energy function, b_{xx}	Unitless	26.6
Exponent of strain energy function, b_{fx}	Unitless	13.3
Maximum peak intracellular Ca concentration, $(Ca_0)_{max}$	µM	4.35
Peak intracellular Ca concentration, Ca_0	µM	4.35
Parameter for isometric tension-sarcomere relationship, B	µm−1	4.75
Sarcomere length at zero-active tension, l_0	µm	1.58
Time to peak tension, t_0	msec	275
Time to beginning of relaxation, t_t	msec	300

3.4 LV Geometry, Meshing and Microstructure of the LV

A normal person and a patient with acute myocardial infarction (AMI) were studied in Singapore's National Heart Center (NHC) to gather clinical data and MR images of the left ventricle [49]. Endocardium surfaces were created based on the MR scans of a normal patient and an AMI patient (Figure 3.3). Based on the reconstructed LV endocardium surfaces, the 3D

LV geometry was built using a half prolate ellipsoid shape. As determined by the clinical data, the LV volume was designed to reflect the minimal pressure state, which lies somewhere between the normal range of ESV and EDV, but close to EDV. Table 3.4 shows the LV models' geometrical parameters. Based on earlier studies [49], the wall thickness of the LV has been modified here. The details of the AMI heart geometry model have been depicted in Figure 3.8, and the extended views of the three different zones of the AMI heart have been illustrated in Figure 3.9.

(a)   (b)
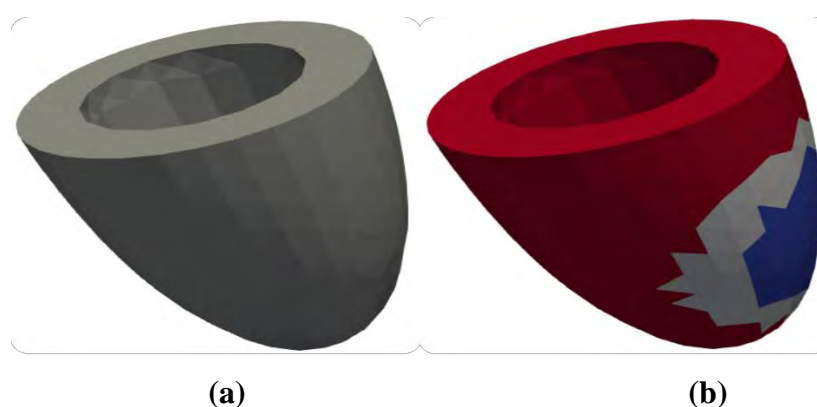
Figure 3. 3: Half prolate ellipsoid geometrical models of LV, constructed based on the acquired MRI images of (a) normal subject and (b) AMI patient.

Table 3. 4: Geometrical Parameters of LV for Normal and AMI baseline model.

	Normal (healthy) heart LV	AMI heart LV
Cavity Diameter (cm) (at basal plane)	4.00	4.00
Length, L (cm)	8.30	8.30
Wall thickness, WT (cm)	1.13	1.13

The discretized LV geometry with 1150 - 1600 quadratic tetrahedral components was created to perform the grid independence test (section 3.5) and is depicted in Figure 3.4. Each quadratic element had a total of ten nodes, each of which had three degrees of freedom (DOF) and could be rotated in three Cartesian coordinate directions. As a result, each quadratic element has a total of 30 degrees of freedom. The myocardial fibers of the left ventricle are organized helically over the length of the ventricle (Figure 3.5). A linear transmural variation was used to vary the helix angle associated with myofiber orientation, which ranged from 60° at the endocardium to -60 ° at the epicardium in the left ventricular (LV) based on existing literature data [50] (Figure 3.6). Because every fiber in the myocardium is intricately

intertwined, deformation occurs as a result of the combined efforts of all the fibers. There are only two types of LV deformation metrics that can be used: (i) three orthogonal components of myocardial deformation (longitudinal shortening, circumferential shortening, and radial thickening), (ii) LV twist (circumferential–longitudinal shear strain resulting from the obliquely arranged double-helical orientation of LV myocardial architecture that greatly enhances the ability to pump blood). The obliquely oriented double-helical orientation of the LV myocardial architecture results in LV twist, which reflects circumferential–longitudinal shear strain and considerably enhances LV ejection (Figure 3.7) [51].
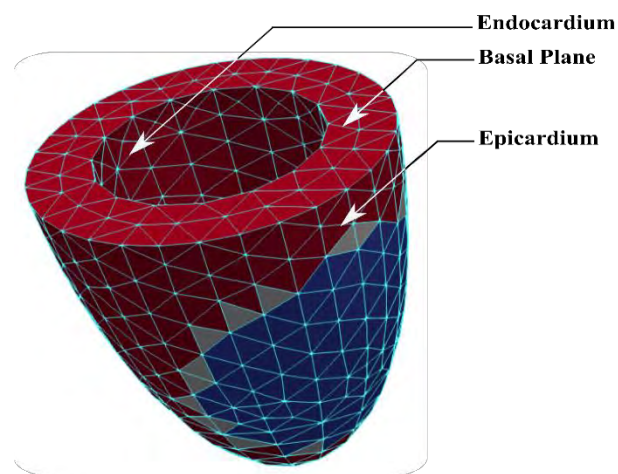
Figure 3. 4: LV geometry defined using a half prolate ellipsoid and discretized with quadratic tetrahedral elements.

(a)   (b)
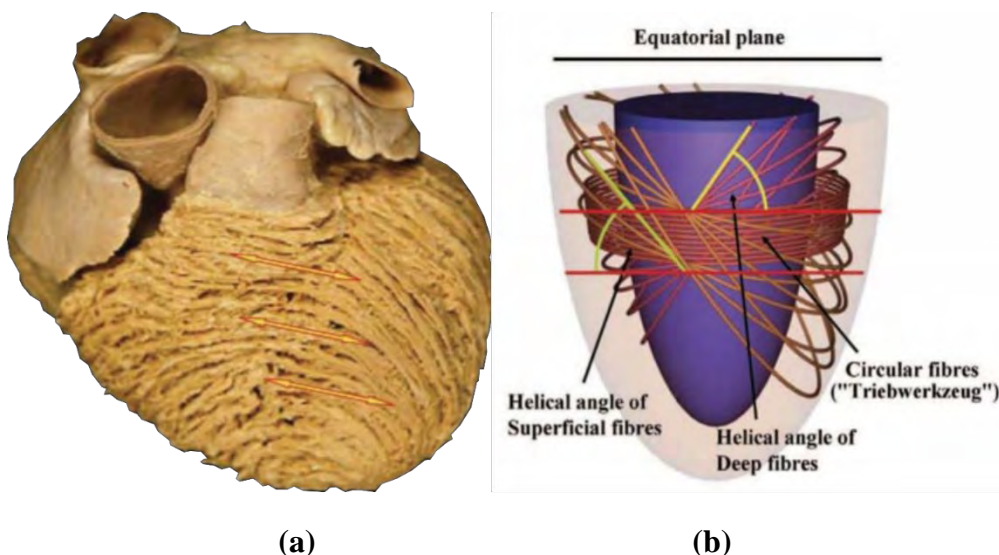
Figure 3. 5: The endocardium to epicardium myofiber direction is shown in (a) a real heart image and (b) a computational model with linear transmural helix angle variation [50].
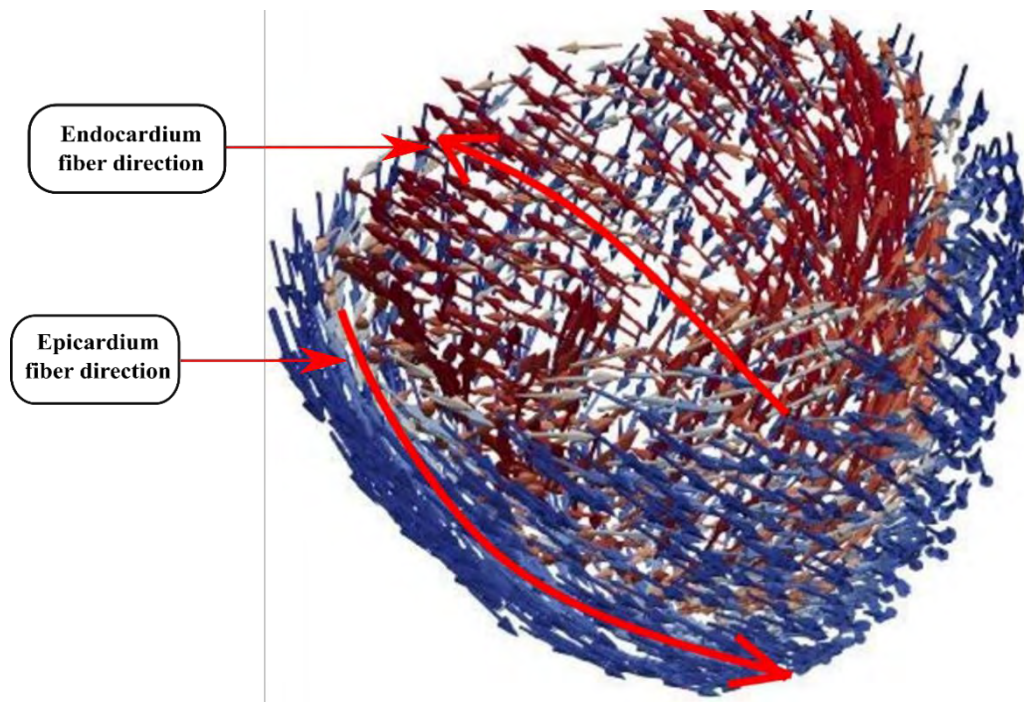
Figure 3. 6: Myofiber path variation by helix angle from the LV endocardium to epicardium in the FE model.
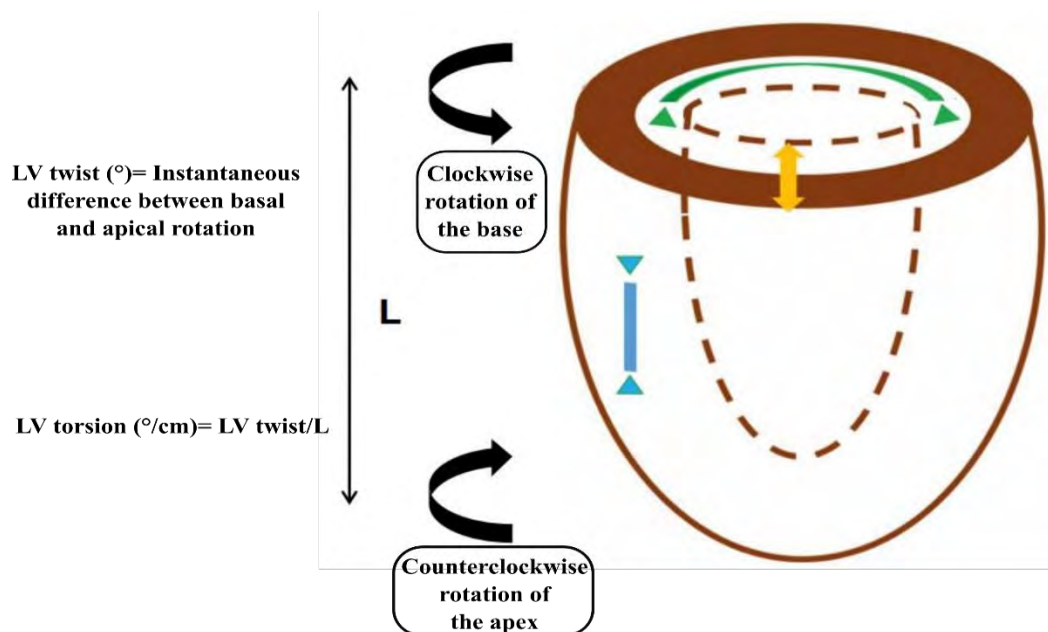
Figure 3. 7: The three orthogonal planes of myocardial deformation are longitudinal shrinking (blue), radial stiffening (orange), and circumferential shortening (green) at systolic condition [50].
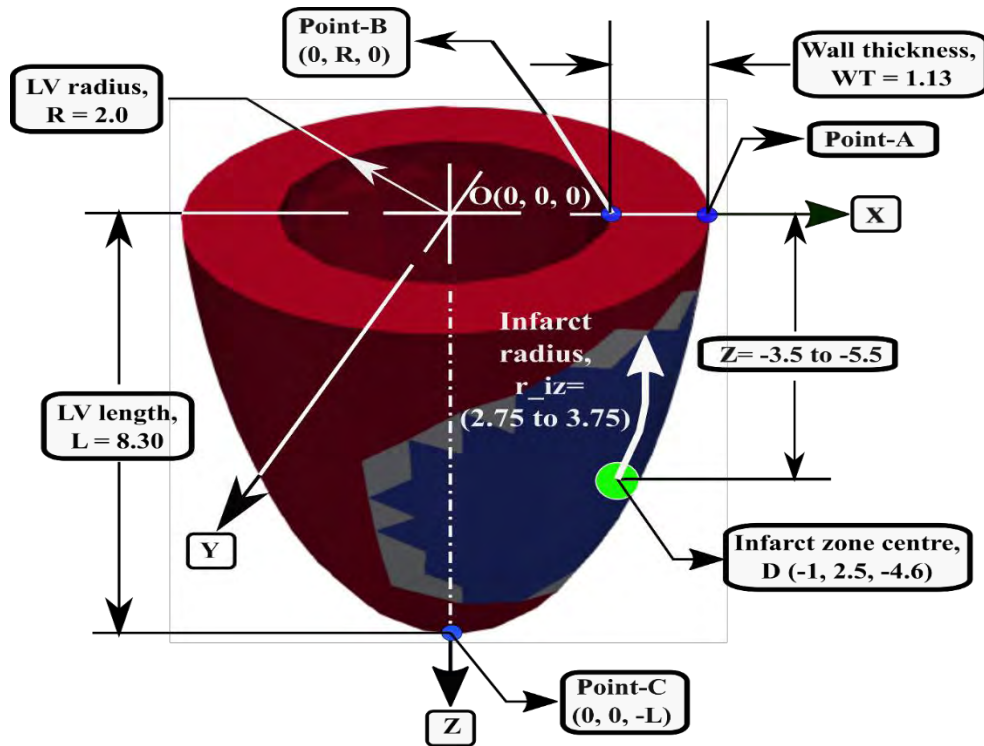
Figure 3. 8: Dimensions of the ellipsoidal LV model of AMI heart geometry with the position of the infarct zone at the center (-1.0, 2.5, -4.6).
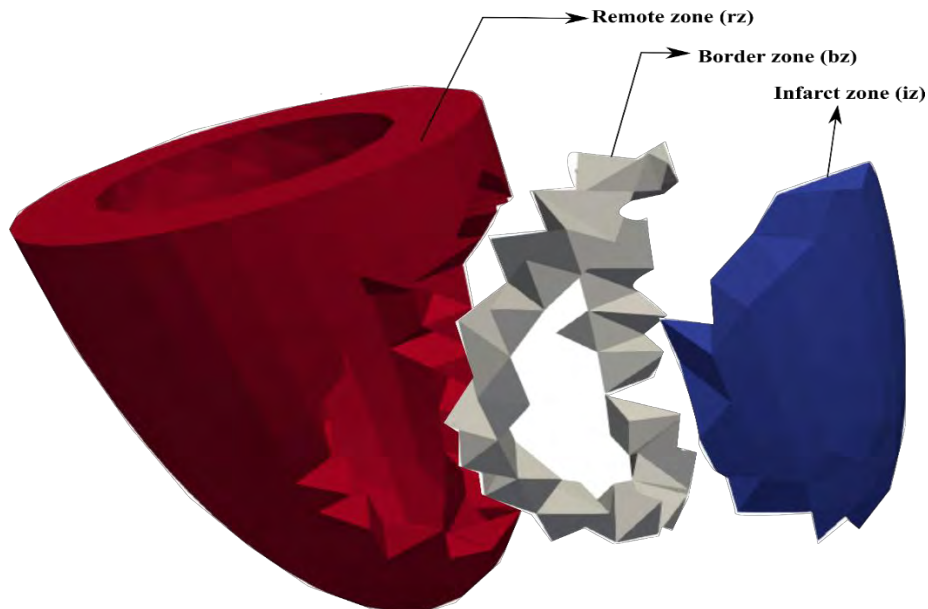
Figure 3. 9: The extended views of the three different zones of the acute myocardial infarction (AMI) LV model: the remote zone (red volume), the border zone (white volume), and the infarct zone (blue volume).

As shown in Figure 3.8, the center of the basal plane has been chosen as the origin (O (0, 0, 0)) point of the AMI LV model, with a total length of L cm between point O and point C (the apex of LV), and a thickness of WT cm between the two points A and B. The infarct

zone center has been identified as the green circle in the blue zone in the figure. In this computational study, four different cases have been studied. Two cases depend on the variations of geometrical parameters such as the position of the infarct zone (Z), and the size of the infarct zone (r_iz). And the other two cases have been performed by varying the LV material properties such as contractility (Tmax), and the stiffness (C) of the infarct zone. To perform the geometrical variations of the infarct zone, the position has been varied in the range of -3.5 cm (upper extreme) to -5.5 cm (lower extreme) along the Z-axis. The size of the infarct zone has been varied by varying the radius of the infarct zone in the range of 2.75 cm to 3.75 cm.

3.5   Grid Independence Test

A grid independence test was done to ensure that the finite element results were consistent with the fluctuation of the number of elements. 350 to 1830 quadratic tetrahedral elements have been run for a baseline case. Figure 3.10 depicts the PV loop, LV volume, and pressure waveforms for a typical LV model with different number of quadratic tetrahedral elements. The maximum pressure difference between 1558 and 1830 elements cases is only ~1.88%. Also, the change in stroke volume between the two cases is about 4.62%. As a result, approximately 1600 elements were selected for the numerical simulation of the various cases in this study to efficiently simulate the cases in terms of simulation time.
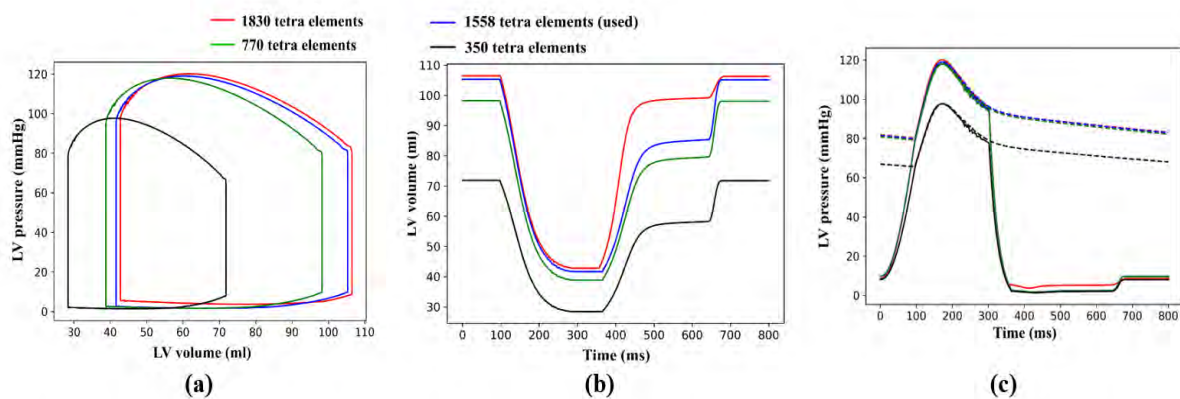
Figure 3.10: Comparison of (a) PV loops, (b) volume waveforms, and (c) pressure waveforms for different number of elements.

CHAPTER 4
RESULTS AND DISCUSSION

The model was calibrated using data obtained from the clinical studies [52, 53] to simulate a healthy subject and an infarct patient (AMI model). With these two models, the model's ability to accurately predict patient-specific characteristics has been demonstrated. Following this, the calibrated AMI model was used to investigate various possible paths of progression by altering relevant parameters. Depending on the type of geometry (infarct size and infarct location), the model parameters for tissue contractility and stiffness were altered. These AMI models with isolated changes in geometry, contractility, or stiffness were compared to the healthy baseline model's results (hemodynamics and overall mechanical behaviors).

4.1 Calibration of the Models: Normal and AMI Case

4.1.1 Comparison between the Model and Clinical Data for the Healthy Subject

The PV loops, pressure, and volume waveforms of the LV for the normal subject predicted by the model were closely matched with the published data [51], as shown in Figure 4.1. The reference EDV (~114 ml) and ESV (~45 ml) were reasonably matched with the model (~109 ml EDV and 43 ml ESV) (Figure 4.1 (a)). As a result, the EF was 61% for the model, which is close to the reference EF of 65% [51] (which is within the normal EF range > 55%) [54]. Pressure waveforms of the LV as shown in Figure 4.1 (b) in the baseline case also showed good agreement with the literature data. The model aortic pressure waveform is within the normal range (systolic < 120 mmHg, diastolic < 80) with an aortic pulse pressure of 40 mmHg (systolic: 120 mmHg, diastolic: 80 mmHg). Figure 4.1 (b) shows that both the model and data represent an approximately equal response for the contraction during the systole and relaxation during the diastole over the cardiac cycle. The key hemodynamic parameters of the calibrated healthy case have been summarized in the Table 4.1.

Table 4. 1: Hemodynamic parameters of the calibrated healthy LV model

Parameter	Unit	Value
End-diastolic volume	ml	109
End-systolic volume	ml	43
Ejection Fraction, EF	%	61
End-systolic pressure, ESP	mmHg	121
End-diastolic pressure, EDP	mmHg	80
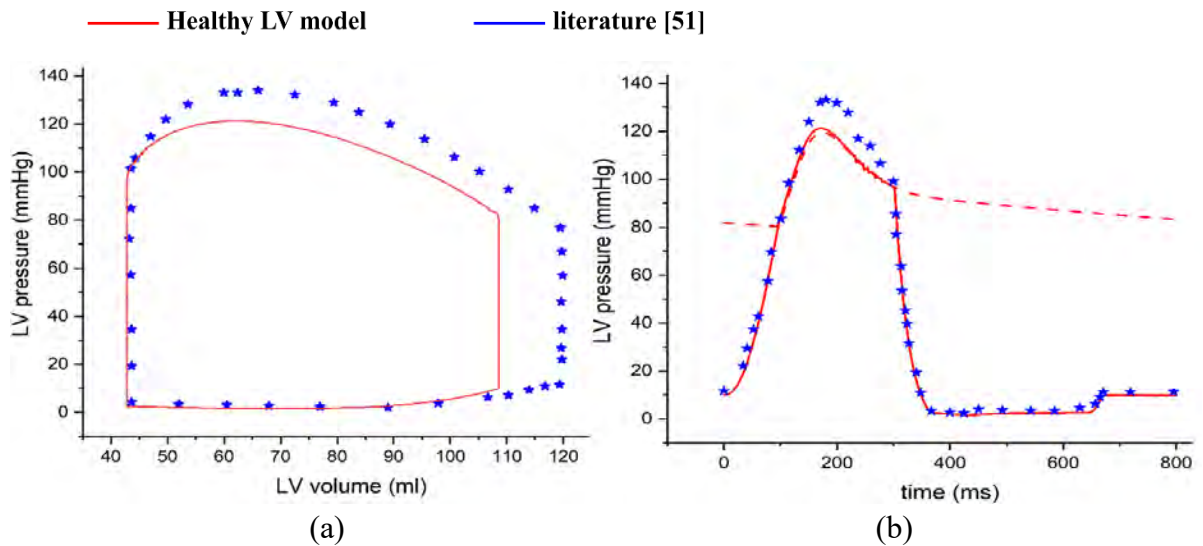
Figure 4. 1: Comparison between the model prediction and literature data [51] for LV (a) PV loops, and (b) pressure waveforms for the healthy subject.

4.1.2 Comparison between the Model and Clinical Data for the AMI Patient
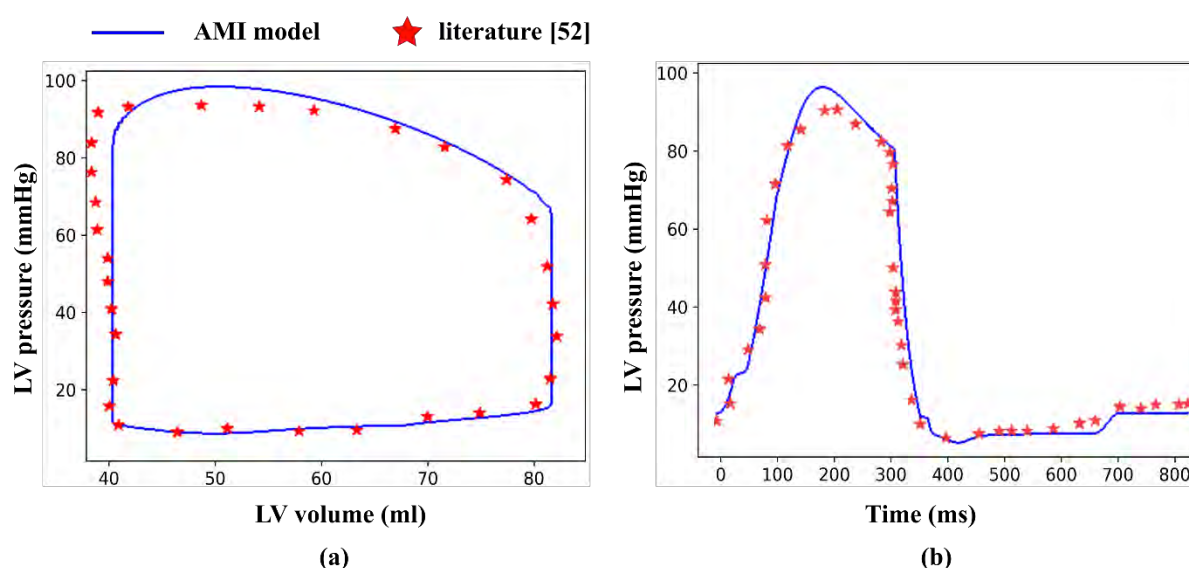
Figure 4. 2: Comparison between the model prediction and clinical data [52] for LV (a) PV loops, and (b) pressure waveforms for the AMI patient.

Similar to the healthy case, the PV loops, pressure, and volume waveforms of the LV for the infarct case (infarct size of ~9% of total LV volume, and the location of infarct at the center (-4.5 cm from the basal plane)) with increased myofiber stiffness of 135 Pa and reduced myofiber contractility of 91 kPa predicted by the model reasonably matched with the clinical data [52] as shown in Figure 4.2. The reference EDV (83 ml) and ESV (39.5 ml) were reasonably matched with the model (83 ml EDV and 40 ml ESV) (Figure 4.2 (a)). As a result, the EF was 52% for the model, which is close to the reference EF of 52.5% (within the heart failure range < 55% [54]). Pressure waveform of the LV as shown in Figure 4.2 (b) in the baseline AMI case also showed good agreement with the clinical AMI data. Similar to the healthy case, the contraction and relaxation phases during the systole and diastole, respectively for the AMI model matched well with the clinical data. All the parameters were kept constant except the myofiber stiffness and contractility of AMI LV model to investigate the effects of infarct zone properties. The changes in myofiber stiffness and contractility in AMI LV model in comparison to the healthy LV model have been tabulated in Table 4.2.

Table 4. 2: Variations in the model parameters of AMI LV in comparison to healthy LV

Parameters	Healthy LV	AMI LV	% change in AMI LV
Stiffness, C (kPa)	125	135	8% ↑
Contractility, Tmax (ms)	130	91	30% ↓
IZ location, z (cm)	-	-4.5	-
IZ radius, r_iz (cm)	-	2.75	-

4.1.3 Comparison of Strains between the Healthy and AMI Cases

The longitudinal strain, Ell (Figure 4.3) and circumferential strain, Ecc (Figure 4.4) profiles have been plotted for the healthy and baseline AMI cases. Clinically, longitudinal and circumferential strains in LV are generally measured using 2D-Doppler and speckle tracking echocardiography (STE) [54]. Typical strain profiles for healthy humans measured in clinics are also shown in Figure 4.3 and Figure 4.4 [54, 55]. For the circumferential strain, the model predicted profiles of healthy and AMI cases were consistent with the measurements found in humans. The simulated circumferential strains of both healthy and AMI cases peak at about 350 ms during systole, which falls in the range of 300 - 450 ms for the clinical measurements. Also, similar to the clinical measurements, a rapid change in the circumferential strain occurs at late diastole at around 650 ms for both cases arising from the contraction of the left atrium. Moreover, the rate of relaxation during the diastole is similar to the clinical measurements for both cases (Figure 4.3). For healthy case, the absolute peak values of circumferential and longitudinal strains are 24% and 22%, respectively, which are reasonably close to the clinical measurements [58]. And, for the AMI baseline case, the absolute peak values of circumferential and longitudinal strains are 17% and 19%, respectively, which have been reduced by 29% and 14%, respectively compared to the healthy case. It has been found that due to the reduction of active zone in the LV having the myocardial infarction, the strain values become impaired and decreased [59]. A clinical trial including 100 patients with 42 AMI patients and 58 healthy subjects demonstrated that the peak Ecc and peak Ell of LV are significantly lower in AMI patients when compared with the healthy subjects [59].
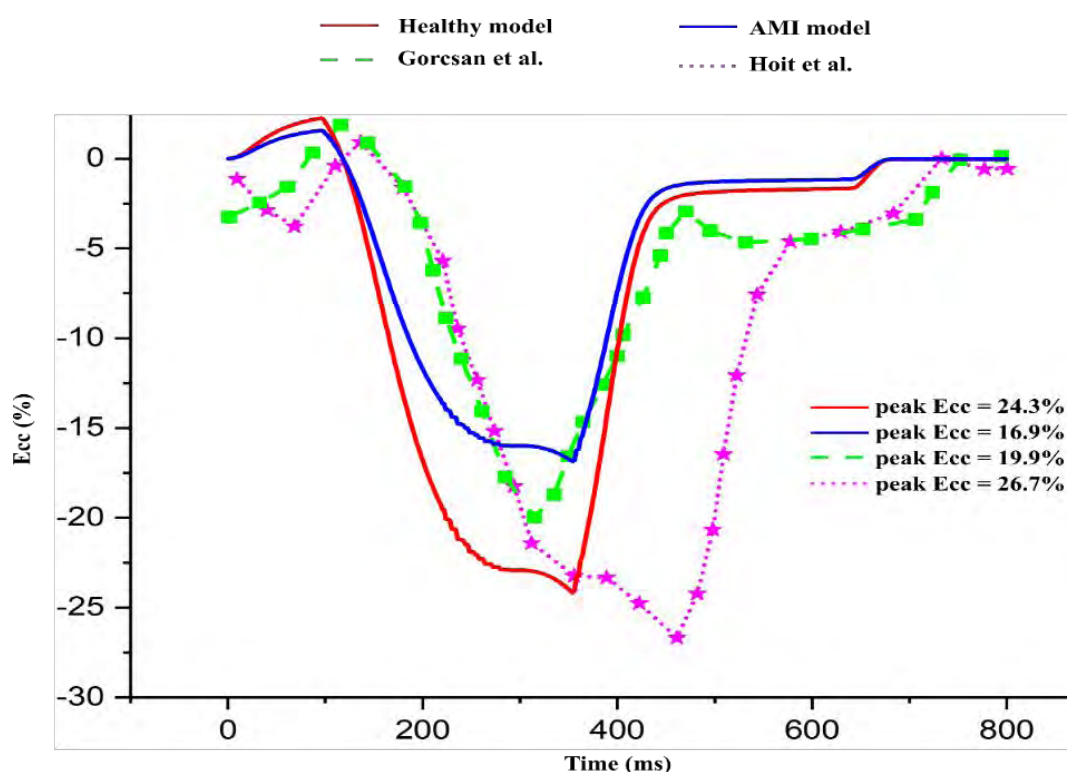
Figure 4. 3: Circumferential strain profiles calculated by the model for healthy and AMI cases compared with healthy echo measurements (dotted pink color [55] and dashed green color [54] lines).

However, studies have also suggested that reduction in peak longitudinal strain in AMI patients are related to the presence of some unrecognized myocardial systolic dysfunction, scar formation, increased rigidity of LV wall, etc., and correlates to the reduction in EF during the progression of this disease [60]. The baseline AMI patient considered in this study has a relatively high EF of 51.6%, which can be a possibility for the model prediction of ~19% peak longitudinal strain which is close to the healthy range. As the disease progresses, the peak longitudinal strain of this AMI patient will eventually decrease significantly compared the healthy subject which will be discussed in the later sections.

4.1.4 Summary

Table 4.3 shows the different hemodynamic and functional indices predicted by the model for healthy and baseline AMI. We can see that the EF is within the normal range for the healthy case, but with the introduction of infarct zone in the LV the EF has been decreased to 52% from 61%. Moreover, both the EDV (83 ml) and ESV (40 ml) of AMI cases have been decreased from the healthy case (109 ml EDV and 43 ml ESV), which is a indication of LV remodeling. The AMI patient has higher end-diastolic pressure (EDP) (~19 mmHg in AMI vs.
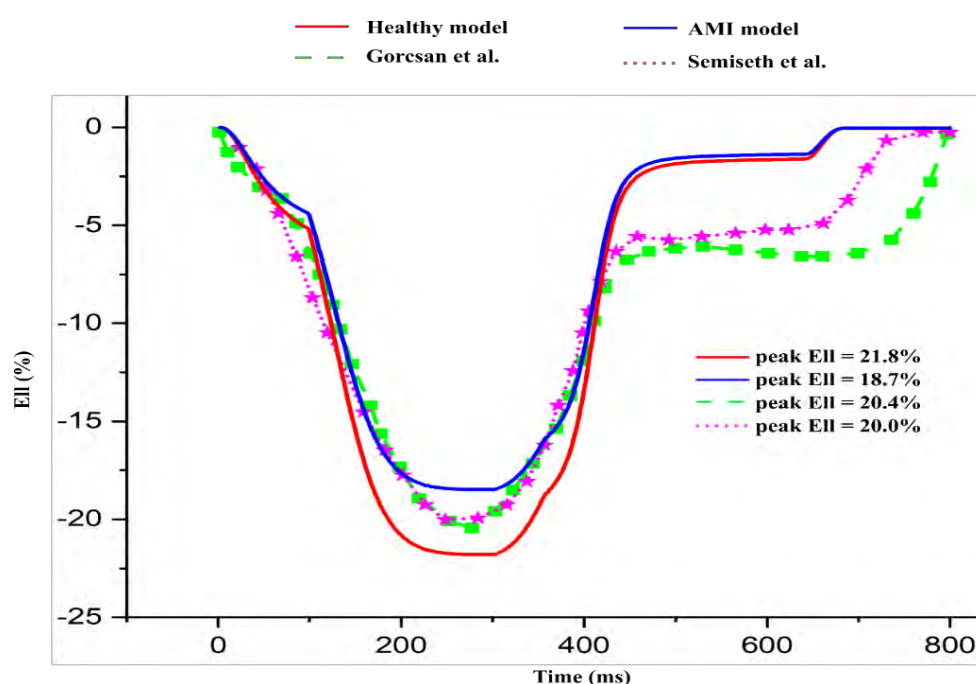
Figure 4. 4: Longitudinal strain profiles calculated by the model for healthy and AMI cases compared with healthy echo measurements (dotted pink color [56] and dashed green color [54] lines)

~16.5 mmHg in normal) than healthy, which suggests AMI patient's LV is stiffer than the healthy LV. Clinically, EDP higher than 12 mmHg is considered a sign of diastolic dysfunction, which is a common feature in AMI [61]. In addition, the absolute peak Ecc and Ell significantly decreased in AMI patients compared to the healthy case, which gives an insight into the impaired LV deformation due to the presence of myocardial infarction. The outcomes of both cases have been summarized in Table 4.3.

Table 4. 3: Model predicted hemodynamic and functional indices for healthy and AMI cases.

Parameters	Healthy case	AMI case	Remarks
End-Diastolic Volume (ml)	109	83	24%↓
Ejection fraction (%)	61	52	15%↓
End-Diastolic Pressure (mmHg)	16.5	19	15%↓
Systolic Blood Pressure (mmHg)	121	98	19%↓
Diastolic Blood Pressure (mmHg)	90	75	17%↓
Peak Circumferential Strain (%)	24.3	17	30%↓
Peak Longitudinal Strain (%)	22	19	14%↓

4.2   Effects of Infarct Size Variations in AMI patient

Managing patients with an acute ST-segment elevation myocardial infarction (MI) necessitates effective risk stratification. In previous studies, acute anterior MI patients had a worse prognosis than non-anterior MI patients because of more pronounced adverse left ventricular (LV) remodeling. As a result, risk assessment algorithms for the prognosis prediction of patients after acute ST-segment elevation MI have included the anterior location of the MI. However, it is still unclear if the worse post-infarction LV remodeling and prognosis associated with anterior MI is due to greater MI size or if infarct location exerts a greater role than MI size. This is a question that needs to be answered [62]. In this modeling study, both the variations have been studied. The rigidity or stiffness of the LV myofiber changes with the introduction of an infarct, and this rigidity or stiffness dramatically increases with the size of the infarct. The geometrical parameters of infarct size that are varied for different cases are tabulated in Table 4.4. Contractility and passive stiffness parameters are shown in Table 4.5 for the AMI cases.

Table 4. 4: Geometrical variations to study the effect of infarct size in AMI patients.

Case ID	Left ventricle volume, LVV (cm^3)	IZ volume, cm^3 (% LVV)	BZ volume, cm^3 (% LVV)	RZ volume, cm^3 (% LVV)	Infarct radius, r_iz (cm)	Infarct location, Z (cm)
Healthy: base		-	-	-	-	-
IZ size-1		9.50 (9%)	13.69 (13%)	82.12 (78%)	2.75	-4.5
IZ size-2	105.28	18.95 (18%)	8.42 (8%)	77.91 (74%)	3.25	-4.5
IZ size-3		28.43 (27%)	3.16 (3%)	73.70 (70%)	3.75	-4.5

*IZ = Infarct Zone, BZ = Border Zone, RZ = Remote Zone

Table 4. 5: Contractility and passive stiffness parameter for the healthy and AMI cases.

Parameters	Unit	Healthy	AMI cases	
Contractility, Tmax	kPa	130	RZ	130
			BZ	104
			IZ	91
Stiffness, C_para	Pa	125	RZ	125
			BZ	125
			IZ	135

*IZ = Infarct Zone, BZ = Border Zone, RZ = Remote Zone

4.2.1 Effects of Infarct Size on LV PV Loop

PV loop, volume waveforms, and pressure waveforms for different infarct size are shown in Figure 4.5 (A), Figure 4.5 (B), and Figure 4.5 (C), respectively. It can be observed from PV loops that both EDV and ESV of LV have been decreased with the increased size of the infarct zone. It can be seen from Figure 4.5 (A) that for the infarct size of 9% (blue), 18% (green), and 27% (black) of LV volume, the EDVs have decreased to 83 ml, 66 ml, and 52 ml respectively from 109 ml EDV of the healthy case (red). And the corresponding ESVs are 40 ml, 35 ml, and 30 ml rather than the healthy ESV of 43 ml. It is also noticeable that the corresponding ejection fractions (EF) of the cases have been decreased consequently to 52%, 47%, and 43% from the healthy case's EF of 61%. For the increased size of the infarct, the contractility of the LV has decreased, while the rate of myocardial relaxation has been increased.

The end-systolic pressure (ESP) has been decreased with the increased infarct size. On the other hand, the end-diastolic pressure (EDP) has been increased with the increased infarct size. The rigidity of the AMI LV rises with the increased infarct size. Therefore, the heart with AMI LV with increased infarct size becomes stiffer than the heart with non-AMI LV. Similar outcomes due to the incremental size of infarct have been suggested and found by Glenn A. H. et al. [63]. The aortic pulse pressure has decreased with the increase of infarct sizes which was
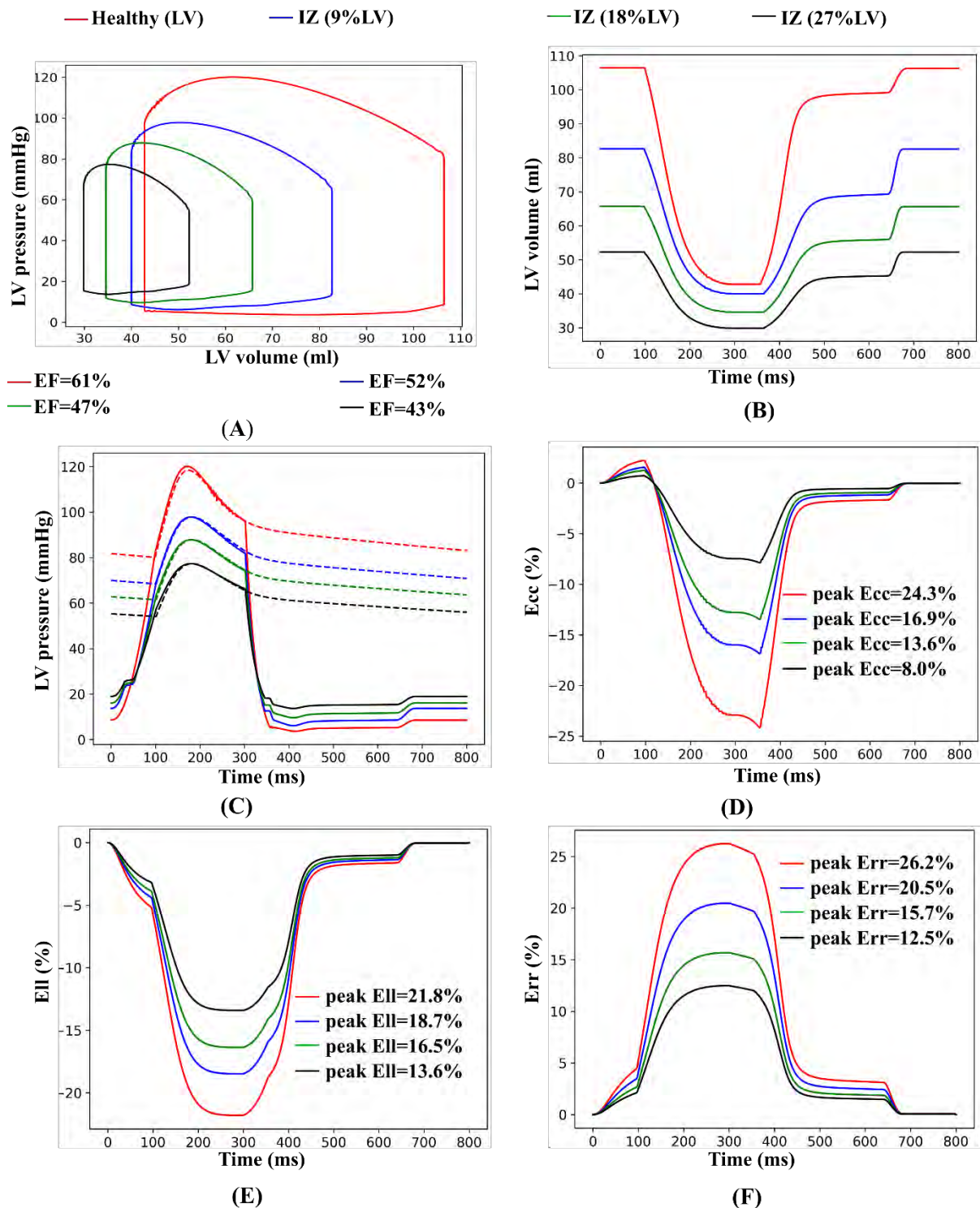
Figure 4. 5: Comparison among LV (A) PV loops, (B) volume waveforms, (C) pressure waveforms, (D) circumferential strains, (E) longitudinal strains, and (F) radial strains at different infarct zone size

about 40 mmHg, 25 mmHg, 20 mmHg, and 15 mmHg for the healthy LV, 9%, 18%, and 27% AMI cases, respectively.

From Figure 4.5 (B), it is obvious that the duration of the isovolumic relaxation phase has increased with the increased size of the infarct. For the healthy LV, the duration of the isovolumic relaxation phase is between 296-364 ms, whether it is between 285-370 ms, 270-378 ms, and 250-385 ms for the infarct size of 9%, 18%, and 27% respectively. This increased duration of the isovolumic relaxation phase also indicates stiffening of LV with the increased volume of infarct size. This result is consistent with the outcomes found by O. Brubakk and K. Overskrid [64]. It is seen in Figure 4.5 (C) that, though the peak LV pressure has been decreased with the increased size of the infarct whereas, the EDP of LV have been increased with the increased infarct size.

4.2.2 Effects of Infarct Size on Strains

The variations of circumferential strain (Ecc), longitudinal strain (Ell), and radial strain (Err) waveforms with the infarct size are shown in Figure 4.5 (D), Figure 4.5 (E), and Figure 4.5 (F), respectively. The significant findings from these figures are that the peak values of Ecc, Ell, and Err are decreasing with the increasing infarct size. The absolute peak Ecc are 17%, 14%, and 8% for the infarct size of 9%, 18%, and 27%, respectively, whereas it is ~24% for the healthy heart (Figure 4.5 (D)). The absolute peak Ell is 19%, 16%, and 14% (Figure 4.5 (E)), and absolute peak Err is 20%, 16%, and 12% (Figure 4.5 (F)), for the infarct size of 9%, 18%, and 27% respectively, whether for healthy case the peak Ell and Err are 22% and 26%, respectively. The reduction in peak strains is consistent with the insights of the infarct size effects on the pressure-volume relations as the remodeling LV becomes stiffer with the scar formation, thrombus effects, or increased hemodynamic loading status caused by myocardial infarction. Similar results of the strains have been found clinically by Mangion et al. [64]. For the 27% increase in infarct zone size, the absolute peak Ecc has been reduced by 67%, absolute peak Ell by 45%, and absolute peak Err by 54% compared to the healthy LV.

The outcomes of pressure, volume, Ecc, Ell, and Err variations due to the infarct size are tabulated in Table 4.6.

Table 4. 6: Model predictions of different LV functional indices for AMI cases with different sizes of infarct zone.

Index	Healthy LV	Infarct Size			Clinical Range for AMI
		9% LVV	18% LVV	27% LVV	
End-diastolic volume, EDV (ml)	109	83	66	52	84.1-121.8 [65]
End-systolic volume, ESV (ml)	43	40	35	30	36.7-69.6 [65]
Ejection fraction, EF (%)	61	52	47	43	49.6±7.5 [65]
End-diastolic pressure, EDP (mmHg)	15	18	18.5	20	11.9±4.6 [66]
End-systolic pressure, ESP (mmHg)	100	90	80	70	99±5 [66]
Absolute peak Ecc (%)	24	17	14	8	13.45±4.1 [65]
Absolute peak Ell (%)	22	19	15	12	20±2.1 [65]
Absolute peak Err (%)	26	20	16	12	14±6 [65]

4.3 Effects of Infarct Location Change in AMI patient

Prognosis after an acute myocardial infarction is heavily influenced by left ventricular dysfunction and infarct size (MI). Anterior myocardial infarction (MI) is associated with a decrease in left ventricular ejection fraction (LVEF) and a worse prognosis [67]. As the infarct location has a significant impact on the infarct size, this parameter may cause the remodeling and dysfunction of LV. Infarction location has a significant impact on the patient's subsequent clinical course. A better prognosis and less myocardial damage can be found in patients with an inferior MI (IMI) compared to those with an anterior MI (AMI) [68]. Very limited research has been performed to find out the effects of infarct locations, and this may create a complicacy for three different directional movements of the infarct zone: radial, circumferential, and

longitudinal. In this study, the positional change of the infarct zone along the radial and circumferential directions has been assumed to be symmetric. Therefore, the longitudinal position along the vertical Z-axis has been considered to investigate the effects of the infarct locations in this study. During this investigation, the infarct size has been kept constant at infarct volume of 9% of LV volume (case: IZ size-1).

The parameters varied in this case are tabulated in Table 4.7, and Table 4.8, respectively. The contractility and passive stiffness were kept same as the infarct volume of 9% of LV volume case (case: IZ size-1).

Table 4. 7: Geometrical variations to study the effect of infarct location towards the basal plane of LV in AMI patients

Case ID	Left ventricle volume, LVV (cm3)	IZ volume, cm3 (% LVV)	Infarct location/center (towards the basal plane)		
			x	y	z
Healthy: base		-	-	-	-
IZ Location-1	105.28	9.50 (9%)	-1	2.5	-4.5
IZ Location-2			-1	2.5	-4.0
IZ Location-3			-1	2.5	-3.5

Table 4. 8: Geometrical variations to study the effect of infarct location towards the apex of LV in AMI patients

Case ID	Left ventricle volume, LVV (cm3)	IZ volume, cm3 (% LVV)	Infarct location/center (towards the apex)		
			x	y	z
Healthy: base		-	-	-	-
IZ Location-1	105.28	9.50 (9%)	-1	2.5	-4.5
IZ Location-2			-1	2.5	-5.0
IZ Location-3			-1	2.5	-5.5

Figure 4. 6: Comparison among LV (A) PV loops, (B) volume waveforms, (C) pressure waveforms, (D) circumferential strains, (E) longitudinal strains, and (F) radial strains at different infarct zone locations towards the basal plane (upward shifting)

4.3.1 Effects of Infarct Location Change towards the Basal Plane (Upward Shifting) on PV Loops

The effects of the change in infarct zone location towards the basal plane (as shown in Table 4.7) on the pressure and volume of LV have been depicted via PV loops, volume waveforms, and pressure waveforms in Figure 4.6 (A), Figure 4.6 (B), and Figure 4.6 (C), respectively. It can be observed from PV loops that both EDV and ESV of LV have been decreased as the infarct zone approaches towards the basal plane. Moreover, the end-systolic pressure (ESP) has been decreased, and the end-diastolic pressure (EDP) has been increased when the infarct zone approaching to the basal plane. The contractility of the LV has decreased while the passive stiffness has increased as the infarct zone approaches towards the basal plane.

It is seen from Figure 4.6 (A) that for the infarct location of $z = -4.5$ cm (blue), $z = -4.0$ cm (green), and $z = -3.5$ cm (black) from the basal plane, the EDVs have been decreased to ~83 ml, 74 ml, and 63 ml respectively from 109 ml EDV of the healthy case (red). And the corresponding ESVs are 40 ml, 38 ml, and 35 ml rather than the healthy ESV of 43 ml. It is also noticeable that the corresponding ejection fractions (EF) of the cases have been decreased consequently to 52%, 49%, and 45% from the healthy case's EF of 61%.

The major observation from these results is that although the changes in pressure and volume are similar to the results found due to the changes in infarct size as described in the previous section, the reduction of the pressure and volume namely, EDV, ESV, EDP, ESP, as well as EF are less compared to the increased infarct size cases. But, for the same infarct size the movement of the infarct location towards the basal plane increase LV stiffness and reduces overall contractile function of the LV. As the more active volume of the LV tends to be affected when the infarct zone moves towards the basal plane, the LV gets stiffer, which is consistent with the findings of Thanavaro et al. [67].

4.3.2 Effects of Infarct Location Change towards the Basal Plane (Upward Shifting) on Strains

The variations of circumferential strain (Ecc), longitudinal strain (Ell), and radial strain (Err) waveforms with the infarct location changes towards the basal plane are shown in Figure 4.6 (D), Figure 4.6 (E), and Figure 4.6 (F) respectively. From these figures, it is seen that the absolute peak Ecc, Ell, and Err are all decreasing with the upward shifting of the infarct zone position. As LV function gets impaired when the infarct zone is moved towards the basal plane

as suggested by the gradual decrease of the EF, these decreasing trends in peak longitudinal and circumferential strains are consistent.

The absolute peak Ecc are 17%, 15%, and 12% for the infarct location (z) of -4.5 cm, -4 cm, and -3.5 cm, respectively, whereas it is ~24% for the healthy heart (Figure 4.6 (D)). The absolute peak Ell are 19%, 16%, and 13% (Figure 4.6 (E)), and absolute peak Err are 20%, 18% and 16% (Figure 4.6 (F)), for the infarct location (z) of -4.5 cm, -4 cm and -3.5 cm respectively, whereas for healthy case the peak Ell and Err are 22% and 26%, respectively. The decrease in peak strains suggests that for same infarct size, the LV function gets more impaired when the infarct location is moved towards the basal plane.

4.3.3 Effects of Infarct Location Change towards the Apex of the LV (Downward Shifting) on PV Loops

The effects of shifting the infarct zone closer to the apex of the LV on the pressure and volume of the LV have been shown in Figure 4.7. As the infarct zone approaches the apex, the ESP and EDP have risen, respectively, whereas the EDP has fallen. The LV's function has improved while its relaxation has decreased in this scenario.

It can be seen in Figure 4.7 (A) that the EDVs have been reduced to 83 ml, 91 ml, and 97 ml, respectively, for the infarct locations of z = -4.5 cm (blue), z = -5.0 cm (green), and z = -5.5 cm (black) from the basal plane compared to the 109 ml EDV of the healthy case (red). Furthermore, the associated ESVs are 40 ml, 41 ml, and 42 ml, rather than the healthy ESV of 43 ml, as shown in the figure. It is also noteworthy that the corresponding ejection fractions (EF) of the instances have fallen as a result, from the healthy case's EF of 61% to 52%, 54%, and 57%, respectively.

The important finding from these simulations is that the results for these cases follows opposite trends compared to those for the upward shifting of infarct locations towards the basal plane. While the upward moving of infarct locations towards the base exacerbates LV dysfunction, downward movement of the infarct zone towards the apex improves LV function. As the infarct zone moves downward, the active volume increases, and the LV stiffness decreases, eventually improving the overall function.
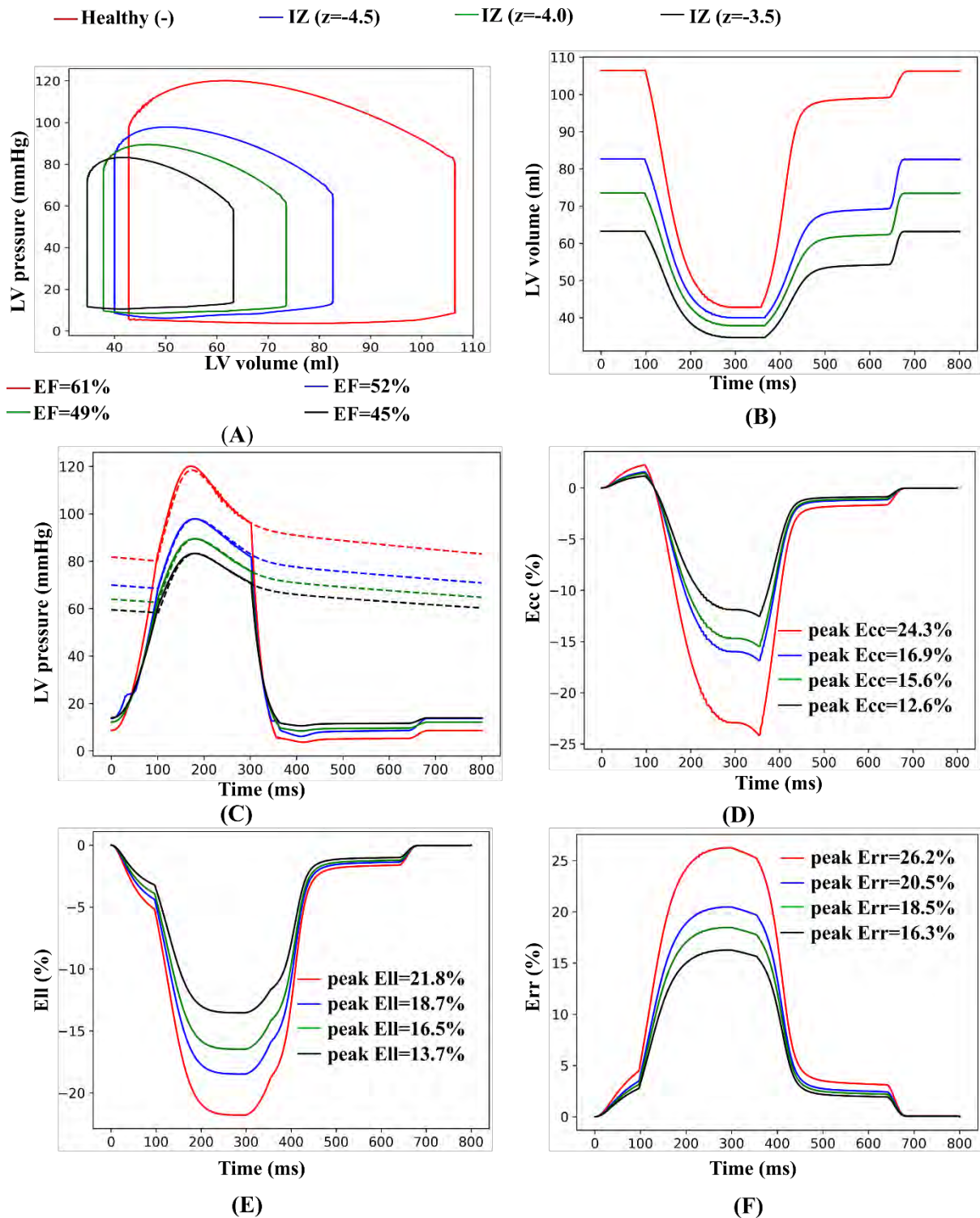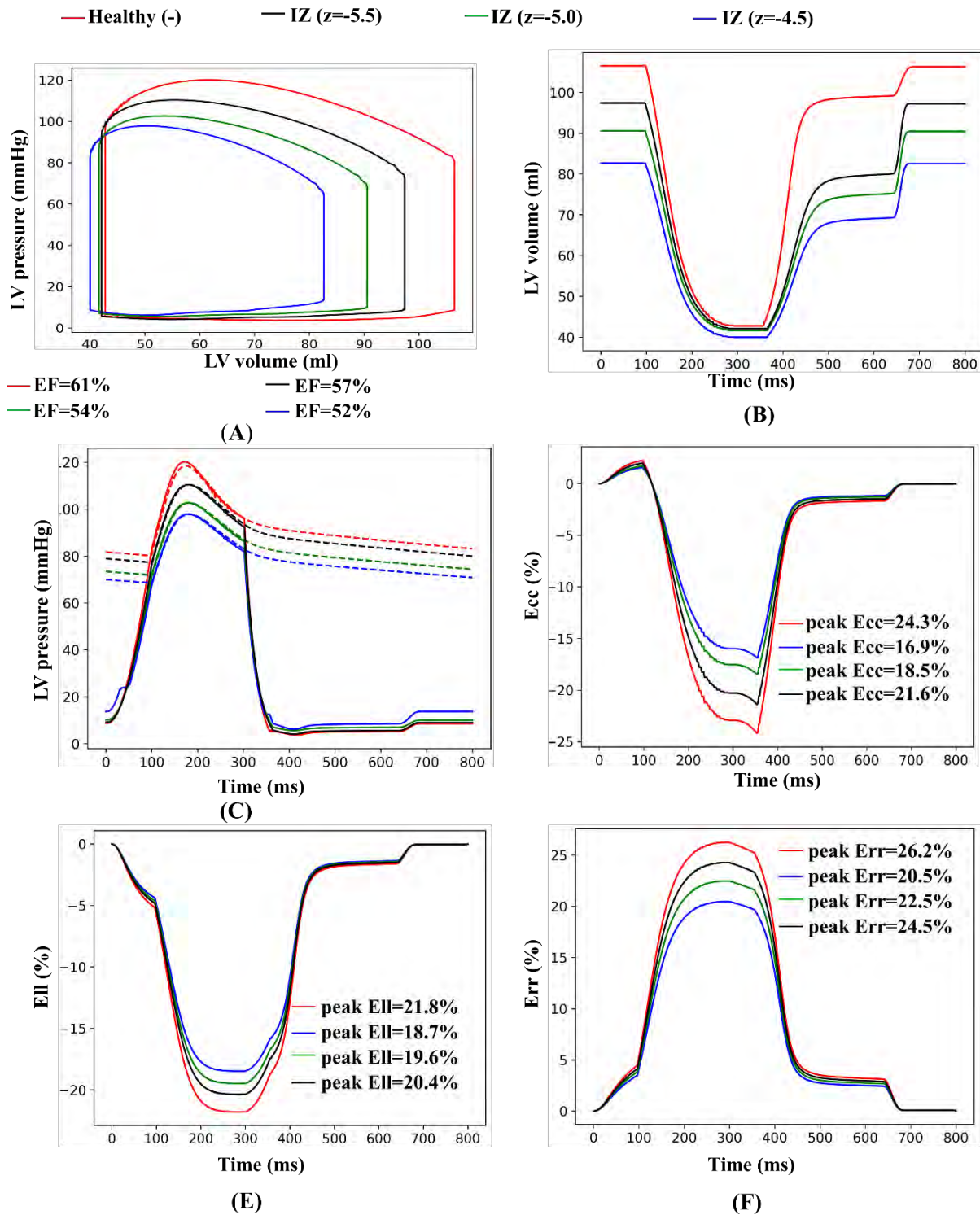
Figure 4. 7: Comparison among LV (A) PV loops, (B) volume waveforms, (C) pressure waveforms, (D) circumferential strains, (E) longitudinal strains, and (F) radial strains at different infarct zone locations towards the LV Apex (downward shifting)

4.3.4 Effects of Infarct Location Change towards the apex (Downward Shifting) on Strains

Circumferential strain (Ecc), longitudinal strain (Ell), and radial strain (Err) waveforms are shown in Figure 4. 7 (D), Figure 4.7 (E), and Figure 4.7 (F), respectively, as the infarct location is moved towards the LV apex. It can be seen from these figures, the absolute peak Ecc, Ell, and Err all increase as the infarct zone position moves downward towards apex.

The absolute peak Ecc values are 17%, 19%, and 22% for infarct locations (z) of -4.5 cm, -4 cm, and -3.5 cm, respectively, compared to 24% for the healthy heart (Figure 4.7 (D)). The absolute peak Ell is 19%, 19.6%, and 20% (Figure 4.7 (E)), and the absolute peak Err is 20%, 22%, and 24% (Figure 4.7 (F)), for infarct locations (z) of -4.5 cm, -5.0 cm, and -5.5 cm, respectively, whereas in the healthy case, the peak Ell and Err are 22% and 26%, respectively. The simulation results of different cases for the movement of infarct location towards base (upward shifting) and apex (downward shifting) are tabulated in Table 4.9.

Table 4. 9: Model predictions of different LV functional indices for AMI cases with different infarct zone locations.

Index	Infarct location (z) (upward shifting) cm		Infarct location (z) (downward shifting) cm			Healthy LV	Clinical Range
	-3.5	-4.0	-4.5 (baseline)	-5.0	-5.5		
End-diastolic volume, EDV (ml)	63	74	83	91	97	109	84.1-121.8 [65]
End-systolic volume, ESV (ml)	35	38	40	41	42	43	36.7-69.6 [65]
Ejection fraction, EF (%)	45	49	52	54	57	61	49.6±7.5 [65]
End-diastolic pressure, EDP (mmHg)	18.5	17.5	18	16.5	15.5	15	11.9±4.6 [66]

Index	Infarct location (z) (upward shifting) cm ←			Infarct location (z) (downward shifting) cm →		Healthy LV	Clinical Range
	-3.5	-4.0	-4.5 (baseline)	-5.0	-5.5		
End-systolic pressure, ESP (mmHg)	75	80	90	95	97	100	99±5 [66]
Absolute peak Ecc (%)	13	16	17	19	22	24	13.45±4.1 [65]
Absolute peak Ell (%)	14	17	19	19.5	20.4	22	20±2.1 [65]
Absolute peak Err (%)	16	18	20	22	24	26	14±6 [65]

4.4 Effects of Change of Stiffness of Infarct Zone in baseline AMI patient case

Myocardial stiffness is believed to be a critical factor in initiating detrimental heart disease [69-70]. After myocardial infarction, ventricular remodeling increases mortality and is strongly linked with the amount of infarct transmurality. Infarct stiffness is predicted to impact regional mechanics and thus the likelihood of human ventricular remodeling. This, however, has not been thoroughly researched [71]. The purpose of this work is to examine the impact of infarct stiffness on myofiber regional mechanics using models from an actively contracting left ventricle. Calculating the appropriate amount of infarct stiffness is necessary to establish balanced regional mechanics across the cardiac cycle, which may be beneficial in therapy, such as myocardial hydrogel injection to regulate its stiffness and lower stress to prevent ventricular remodeling [71]. This case of stiffness change has been performed using the AMI geometry model with 9% of infarct volume (case: IZ size1), and infarct location of z = -4.5 cm (case: IZ Location1). The parameters varied in this experiment are tabulated in Table 4.10. The contractility and passive stiffness were kept constant during this study as shown in Table 4.5.

Table 4. 10: Variations in stiffness parameter of Infarct zone to investigate the effects in baseline AMI patients.

Case ID	Stiffness, C (Pa)		
	Remote zone (RZ)	Infarct zone (IZ)	
	C (Pa)	C (Pa)	% increase compare to remote zone (unaffected)
Healthy: base (C)	125	125	0
IZ_C1	125	135	8
IZ_C2	125	145	16
IZ_C3	125	155	24

4.4.1 Effects of Stiffness Change on PV Loop

The effects of the change in cardiac tissue stiffness (as shown in Table 4.11) on the pressure and volume of LV have been represented in Figure 4.8 (A), Figure 4.8 (B), and Figure 4.8 (C), respectively, using PV loops, volume waveforms, and pressure waveforms. As with the behavior of the infarct size and infarct locations (upward shifting), the PV loops demonstrate that when infarct zone stiffness increases, both EDV and ESV of the LV decrease. Additionally, the end-systolic pressure (ESP) was decreased while the end-diastolic pressure (EDP) was increased as the infarct zone stiffness increased. As infarct zone stiffness increases, the remodeling LV's contractility decreases, and its stiffness increases.

It is seen from Figure 4.8 (A) that the EDV has been decreased to 62 ml (IZ_C3 case: black) from 109 ml EDV of healthy LV (red). And the corresponding ESV is 34 ml, while for healthy LV, the ESV is 43 ml. The EF has also decreased due to the increasing IZ stiffness. For the extreme most case of stiffness (IZ_C3 case), the lowest EF was achieved, and it is 44% for this case reduced from 61% EF of healthy. It can be said from Figure 4.8 (C) that the peak LV pressure for the case of IZ_C3 is higher than the peak pressure of infarct size case of 27% (IZ size-3) (Figure 4.5 (C)), from where it is clear that the effects of stiffness are less than the effects of infarct size on the LV pressure. These findings are consistent with the results investigated by C. Leong et al. [70].
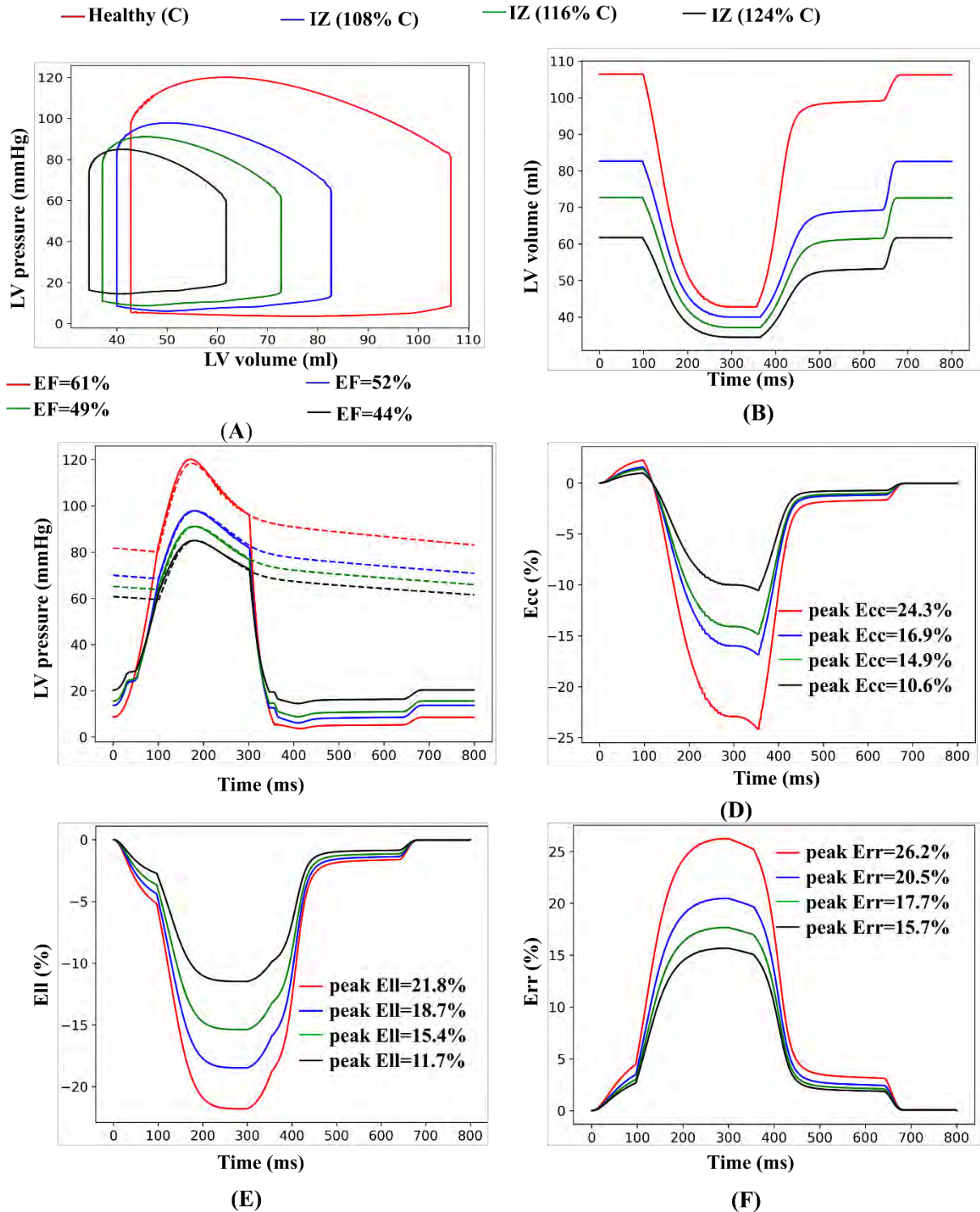
Figure 4. 8: Comparison among LV (A) PV loops, (B) volume waveforms, (C) pressure waveforms, (D) circumferential strains, (E) longitudinal strains, and (F) radial strains at different infarct zone stiffness (parameter 'C' of the model)

4.4.2 Effects of Stiffness change on Strains

Circumferential strain (Ecc), longitudinal strain (Ell), and radial strain (Err) waveforms are shown in Figure 4.8 (D), Figure 4.8 (E), and Figure 4.8 (F), respectively, as a function of myocardial stiffness. As can be seen from these figures, the effects of stiffness changes are similar to the effects of infarct size and location variations described in sections 4.2.2 and 4.3.3, respectively. Though the strains are decreasing with the increase in fiber stiffness, the decreasing rate is comparatively less than that found in the cases of infarct size and infarct location.

The absolute peak Ecc for the stiffness cases of IZ_C1, IZ_C2, and IZ_C3 are 17%, 15%, and 11%, respectively, whereas the healthy heart has a peak Ecc of 24% (Figure 4.8 (D)). For the cases, the absolute peak Ell is 19%, 15%, and 12% (Figure 4.8 (E)), and the absolute peak Err is 20%, 18%, and 16% (Figure 4.8 (F)), whereas the peak Ell and Err are 22% and 26% for healthy patients, respectively. The findings of the stiffness change effects on strains are consistent with the pressure-volume relationships as the remodeling LV stiffens due to myocardial dysfunction and increased hemodynamic loading status, which promotes the stiffness of the infarct zone. For the 20% increase in infarct zone stiffness, the absolute peak Ecc has been reduced by 54%, absolute peak Ell by 45%, and absolute peak Err by 38% in comparison to the healthy LV.

The outcomes of pressure, volume, Ecc, Ell, and Err variations due to the change in infarct zone stiffness are tabulated in Table 4.11.

Table 4. 11: Model predictions of LV functional indices for the variation of stiffness of the infarct zone in baseline AMI case.

Index	Healthy LV	Infarct zone stiffness			Clinical
	125 Pa	135 Pa	145 Pa	155 Pa	Range
End-diastolic volume, EDV (ml)	109	83	73	62	84.1-121.8 [65]
End-systolic volume, ESV (ml)	43	40	37	34	36.7-69.6 [65]
Ejection fraction, EF (%)	61	52	50	44	49.6±7.5 [65]

Index	Healthy LV	Infarct zone stiffness			Clinical Range
	125 Pa	135 Pa	145 Pa	155 Pa	
End-diastolic pressure, EDP (mmHg)	15	18	18	20	11.9±4.6 [66]
End-systolic pressure, ESP (mmHg)	100	90	85	78	99±5 [66]
Absolute peak Ecc (%)	24	17	14	11	13.45±4.1 [65]
Absolute peak Ell (%)	22	19	15	12	20±2.1 [65]
Absolute peak Err (%)	26	20	18	16	14±6 [65]

4.5 Effects of change of Contractility in AMI patient

Myocardial infarction (MI) is a condition that results in heart failure (HF) and early death. The relative contributions of myocyte mortality and decreased myocyte contractility to the induction of HF following MI are unknown and are one of the major subjects of this study. Vascular disease can result in a cessation of the heart's blood supply (myocardial infarction [MI]). The consequent decrease in contractile mass results in an immediate decrease in ventricular pump function [72].

Currently, the most frequently used method in clinical practice for assessing left ventricular (LV) systolic function is to estimate LV ejection fraction (LVEF) using either direct measurements of ventricular volumes during cardiac catheterization or two-dimensional echocardiography [73]. LVEF expresses ventricular ejection (stroke volume, SV) as a fraction of preload (end-diastolic volume, EDV). LVEF is a significant independent predictor of mortality in patients with heart failure and acute myocardial infarction and is critical for treatment decision-making. LVEF, on the other hand, is an imprecise indicator of LV intrinsic contractility, as it is greatly influenced by LV loading conditions. For example, the LVEF's capacity to detect LV systolic failure in septic shock patients has been questioned recently. Even in the context of severely reduced LV intrinsic contractility, a normal LVEF accompanied with a profoundly decreased arterial tone, as described in sepsis, can be detected [73].

As the presence of myocardial infarction adversely affects the contractility of the LV tissue, the contractility variations have also been taken into consideration in this study to investigate its effect on the LV pressure-volume behavior, and on the myocardial strain development. This case of contractility change has been performed using the AMI geometry model with 9% of infarct volume (case: IZ size1) and infarct location of z=-4.5 cm (case: IZ Location-1). The parameters varied in this experiment are tabulated in Table 4.12. The contractility and passive stiffness were kept constant during this study as shown in Table 4.5.

Table 4. 12: Variations in contractility parameter to investigate the effects in AMI patients.

| Case ID | Contractility, Tmax (kPa) | | |
| | Remote zone (RZ) | Infarct zone (IZ) | |
	Tmax, RZ (kPa)	Tmax. IZ (kPa)	% decrease compare to Tmax, RZ
Healthy: base (C)	130	130	0
IZ_C1	130	91	30.00
IZ_C2	130	65	50.00
IZ_C3	130	39	70.00

4.5.1 Effects of Contractility Change on PV Loop

Figures 4.9 (A), 4.9 (B), and 4.9 (C) illustrate the PV loop, volume waveforms, and pressure waveforms, respectively, as a function of contractility of myocardial tissue of the infarct zone. Unlike in the other situations discussed in the previous sections, contractility changes in PV loops do not appear to have similar effects. Even though the ESV has been increased, the EDV has been decreased because of the decreased contractility. Due to reduced contractility, despite an increase in ESV, the ejection fractions have decreased. As the decreased contractility of the infarct zone makes the AMI LV more flexible, and the more permanent deformation develops in the LV fiber, the LV with AMI becomes dilated-for what though the EDV has been decreased, the ESV has been increased.

Contradictory to the effects of contractility on the volume, the pressure behaves as similar to the other cases. In this case, the ESP has been decreased, and the EDP has been increased with the decreased contractility. Similar insights on the pressure outputs were found in the cases of increased infarct size, infarct location, and stiffness. The effects of contractility on the pressure and volume are consistent with the findings investigated by Monge García et al. [72].
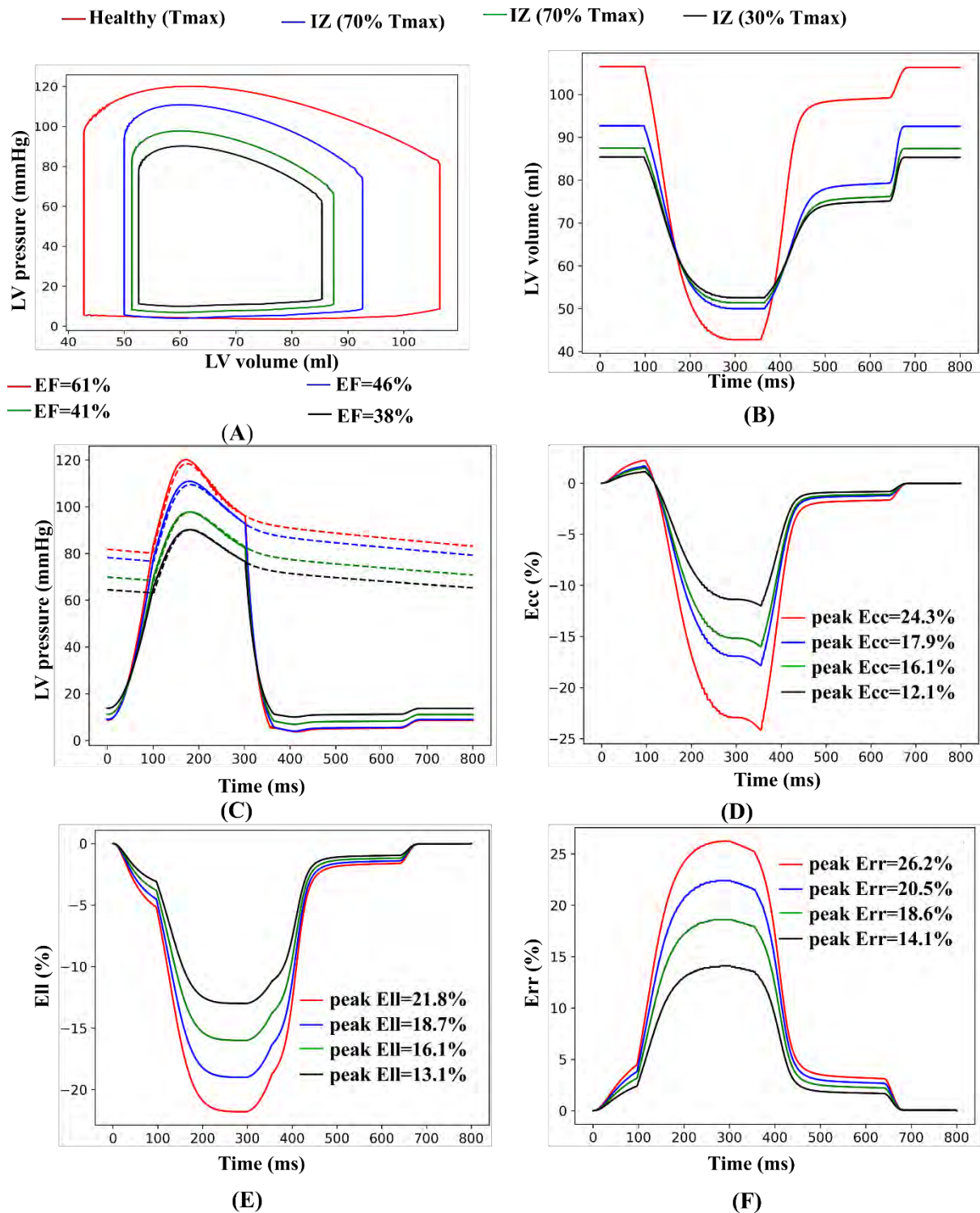
Figure 4. 9: Comparison among LV (A) PV loops, (B) volume waveforms, (C) pressure waveforms, (D) circumferential strains, (E) longitudinal strains, and (F) radial strains at different infarct zone contractility (Tmax)

4.5.2 Effects of Contractility change on Strains

Circumferential strain (Ecc), longitudinal strain (Ell), and radial strain (Err) waveforms are shown in Figure 4.9 (D), Figure 4.9 (E), and Figure 4.9 (F), respectively, as a function of myocardial stiffness. The peak Ecc, peak Ell, and peak Err have decreased with the decreased contractility. When myocardial tissue becomes damaged due to infarction, the heart becomes dilated, and the pumping capacity of the LV has been affected adversely [35]. Figure 4.9 (E) indicates that the effects of contractility are mild on the longitudinal strains, whether it is severe on the circumferential or radial strains. For the 70% reduction in infarct zone contractility, the absolute peak Ecc has been reduced by 50%, absolute peak Ell by 40%, and absolute peak Err by 46% compared to the healthy LV.

The outcomes of pressure, volume, Ecc, Ell, and Err variations due to the change in infarct zone contractility are tabulated in Table 4.13.

Table 4.13: Model predictions of LV functional indices for the variation of contractility of the infarct zone in baseline AMI case.

Index	Healthy LV	Infarct zone contractility			Clinical Range
	130 kPa	91 kPa	65 kPa	39 kPa	
End-diastolic volume, EDV (ml)	109	93	87	85	84.1-121.8 [65]
End-systolic volume, ESV (ml)	43	50	51	53	36.7-69.6 [65]
Ejection fraction, EF (%)	61	52	42	38	49.6±7.5 [65]
End-diastolic pressure, EDP (mmHg)	15	17	17.5	18	11.9±4.6 [66]
End-systolic pressure, ESP (mmHg)	100	90	85	80	99±5 [66]
Absolute peak Ecc (%)	24	18	16	12	13.45±4.1 [65]
Absolute peak Ell (%)	22	19	16	13	20±2.1 [65]
Absolute peak Err (%)	26	20	19	14	14±6 [65]

4.6 Summary

Myocardial infarction (MI) is a life-threatening illness leading to heart failure (HF) and premature death. Vascular disease can result in the heart's blood supply being cut off (myocardial infarction [MI]). Due to the appearance of myocardial tissue damage known as MI, the infarct zone volume progresses with time without proper clinical assessment. With the progression in infarct size, it is seen that the heart becomes stiffens gradually, and pumping capacity falls with the reduced ejection fractions. Similar trends of progression of LV dysfunction have been observed in the cases of upward shifting of the infarct location where the active region of LV was affected severely, and in consequence, the rigidity or stiffness were increasing. For the decrease in the active region of LV, the pumping capacity or the ejection fractions have been decreased in this case of upward shifting of the infarct zone. But, in contrast to the infarct size and infarct location (upward shifting), the opposite impacts have been observed where the ejection fractions were increasing with the downward moving of the infarct zone. With the downward moving of the infarct zone, the active region increases, and the LV behaves like a healthy heart LV.

As mentioned earlier, the infarct size affects the LV and promotes the progression of LV dysfunction, which increases the stiffness and decreases the contractility of myocardium tissue. For same infarct size gradually increasing the tissue stiffness worsens the overall LV function. On the other hand, gradually decreasing the tissue contractility for the same infarct size impairs the overall LV function. Clinically it is much easier to assess the infarct size and location whereas it is very difficult to quantify the tissue stiffness or contractility (myocardial wall properties). The results of this study devise a possible way to quantify these properties by matching the clinical measurements of the AMI patient which could be helpful to plan the course of clinical therapies.

CHAPTER 5
CONCLUSION

5.1 Conclusions

In this thesis, a coupled LV FE-lumped parameter circulatory modeling framework has been calibrated to model the acute myocardial infarction (AMI) patients. The baseline AMI model was successfully matched with the clinical data from the literature by calibrating the different model parameters. The calibrated AMI model was used to study the effects of infarct size and location, stiffness, and contractility on the left ventricular function. The findings of this study are summarized below:

- Increasing the infarct size adversely effects the left ventricular function and gradually progress towards more acute heart failure (HF). Increased infarct size means less active zone of LV, therefore, the LV function as indexed by EF gradually decreases. In addition, the peak longitudinal and circumferential strains decreased with the increase of infarct size. However, the decrease of peak circumferential strain was more severe than the longitudinal strain which suggests that the LV's ability of circumferential shortening was more severely affected than the longitudinal shrinking.

- The active LV volume is adversely affected due to the presence of scar formation or thrombus formation in myocardial infarction. It is seen that for the same size of infarct region, the active heart volume was drastically reduced for the moving of the infarct zone towards the basal plane (upward shifting), however, the reverse effects have been observed when the infarct zone movement was towards the LV apex (downward shifting). For the closest position of the infarct zone towards the basal plane ($z = -3.5$ cm) the EF, ESP, absolute peak Ecc, absolute peak Ell, and absolute peak Err have been reduced by 26%, 25%, 45%, 36%, and 38% from the healthy case, whether for the nearest position to the apex ($z = -5.5$ cm) the reduction of the corresponding parameters were 6%, 3%, 8%, 7%, and 7% which were small compared to the location of $z = -3.5$ cm. From these results, it can be concluded that the LV function is more severely affected when the infarct zone moves towards the LV base for the same size of infarct.

- For a particular infarct size, if the myocardial stiffness is increased then it has been found that for the 30% increase in myocardial stiffness the EDV, and ESV have been reduced by 43%, and 21% respectively, and the corresponding EF has been decreased by 28% which is approximately equal to the effects of the increased infarct size of 27% LVV (EF decreased by 29%).

- For the same infarct size, reduction in contractility increased the end-systolic volume (ESV) and the decreased the end-diastolic volume (EDV). The EF and peak longitudinal and circumferential strains have decreased. With decreased contractility, gradually the LV function becomes weaker and progress towards more acute heart failure.

- The variations of tissue stiffness and contractility for same infarct size have significant effects on the overall LV function which suggests that it is important to quantify these tissue properties in the infarct zone. However, clinically it is very difficult to quantify these properties. But, as shown in this study it is possible to vary these properties in the model to match the clinical data of AMI patients to quantify the tissue stiffness and contractility which can be useful to devise the therapies such as, aspirin, hydrogel injection, or drugs injection etc. to improve the myocardial wall properties such as contractility and stiffness.

- The simulation results of this thesis work demonstrate that by proper development of FE formulation with realistic LV geometry and appropriate tissue constitutive relations can help to understand the underlying mechanics of LV deformation particularly by quantifying the global LV strain profiles for diseases such as, myocardial infarction.

5.2   Limitations of the Work

While it has been demonstrated that the model can reasonably reproduce the results found in the literature, the model does have some limitations. These are discussed below:

- LV was modeled through the use of idealized geometry. LV's approximated half-prolate geometry omitted asymmetrical geometrical characteristics.

- The model assumes that the left ventricle contracts uniformly and ignores any regional activation patterns.

- In this model, a rule-based myofiber orientation was specified in which the myofiber helix angle varied linearly from endocardium to epicardium. In actuality, the orientation of myofibers may be more complex.

- Mechanical effects of the right ventricle (RV) and pulmonary circulation were disregarded. Although the cavity pressure in the RV is significantly smaller than that in the LV, its presence may have an effect on the LV mechanics via the septum.

- Due to the mathematical formulation's omission of the fluid's dynamic behavior and interaction with the vessel wall, this study did not investigate the spatial variation of the pressure waveform along the left ventricle's regions.

- Finally, because the pathophysiology of HF caused by AMI is not well defined, the proper connection between physiological alterations and the progression of AMI is imprecisely characterized. Additional clinical research is required to determine the optimal AMI progression pathway.

5.3 Recommendation for Future Works

The current model, as previously described, has some drawbacks. The current model can be improved upon, and further research can be conducted. These include the following:

- A more realistic model derived from an MRI scan of the human heart can be utilized to ensure that the findings fit the measured clinical data more precisely.

- Rather than employing the electrical analog solely, finite element models of other storage compartments such as the aorta and left atrium can be included with the existing left ventricle model.

- The model can be used in conjunction with fluid dynamics to explore blood pressure and velocity variation as it flows through distinct compartments.

- The model must be revised regularly to incorporate discoveries, as the mechanism of HF caused by AMI is still a subject of current research. With time, researchers are investigating new horizons in this discipline.

REFERENCES

[1] Virani, S. S. *et al.,* "*Heart disease and stroke statistics—2020 update: A report from the American Heart Association.*" *Circulation* (2020). doi:10.1161/CIR.0000000000000757.

[2] Burkhoff, D., "Mechanical Properties of the Heart and Its Interaction with the Vascular System." Card. Physio., vol. 84, pp. 1-23, 2002.

[3] Reimer, K. A., Jennings, R. B. & Tatum, A. H., "Pathobiology of acute myocardial ischemia: Metabolic, functional and ultrastructural studies." *Am. J. Cardiol.* 52, 72–81 (1983).

[4] Frangogiannis, N. G., "Pathophysiology of myocardial infarction." *Compr. Physiol.* 5, 1841–1875 (2015).

[5] Thygesen, K. *et al.,* "Fourth universal definition of myocardial infarction (2018)." *Kardiol. Pol.* 76, 1383–1415 (2018).

[6] Mendis, S. *et al.,* "World Health Organization definition of myocardial infarction: 2008-09 revision." *Int. J. Epidemiol.* 40, 139–146 (2011).

[7] Thygesen, K. *et al.,* "Third universal definition of myocardial infarction." *Eur. Heart J.* 33, 2551–2567 (2012).

[8] Glass, L., McCulloch, A., Hunter, P. (1991), "Theory of Heart: Biomechanics, Biophysics, and Nonlinear Dynamics of Cardiac Function." Springer-Verlag New York, Inc., New York, USA.

[9] Guyton, A. C., Hall, J. E. (1996), Textbook of medical physiology. 9th ed. Philadelphia: W.B. Saunders., USA.

[10] Tanné, D., Bertrand, E., Kadem, L., Pibarot, P. & Rieu, R., "Assessment of left heart and pulmonary circulation flow dynamics by a new pulsed mock circulatory system." Exp. Fluids 48, 837–850 (2010).

[11] de Pater, L. & van den Berg, J., "An electrical analogue of the entire human circulatory system." *Med. Electron. Biol. Eng.* 2, 161–166 (1964).

[12] Hauck, A., Porta, N., Lestrud, S. & Berger, S., 'The pulmonary circulation in the single ventricle patient.' *Children* 4, 1–12 (2017).

[13] Noordegraaf, A. V. *et al.,* "Pathophysiology of the right ventricle and of the pulmonary circulation in pulmonary hypertension: An update." *Eur. Respir. J.* 53, (2019).

[14] Movahed, A., Gnanasegaran, G., Buscombe, J. R. & Hall, M., "*Integrating cardiology*

for nuclear medicine physicians: A guide to nuclear medicine physicians. Integrating Cardiology for Nuclear Medicine Physicians: A Guide to Nuclear Medicine Physicians (2009)." doi:10.1007/978-3-540-78674-0.

[15]   Luisada, A. & MacCanon, D. M., "Fundamentals of clinical cardiology: The phases of the cardiac cycle." *Am. Heart J.* 83, (1972).

[16]   Santhanakrishnan, A., Okafor, I., Kumar, G. & Yoganathan, A. P., "Atrial systole enhances intraventricular filling flow propagation during increasing heart rate." *J. Biomech.* 49, 618–623 (2016).

[17]   Pelech, A. N., "Murmurs. *Nelson Pediatr. Symptom-Based Diagnosis."* 116-143.e2 (2018) doi:10.1016/B978-0-323-39956-2.00008-X.

[18]   Pasipoularides, A., "Right and left ventricular diastolic pressure-volume relations: A comprehensive review." *J. Cardiovasc. Transl. Res.* 6, 239–252 (2013).

[19]   Mehrzad, R., Rajab, M. & Spodick, D. H., "The three integrated phases of left atrial macrophysiology and their interactions." *Int. J. Mol. Sci.* 15, 15146–15160 (2014).

[20]   Iyngkaran, P., Anavekar, N. S., Neil, C., Thomas, L. & Hare, D. L., "Shortness of breath in clinical practice: A case for left atrial function and exercise stress testing for a comprehensive diastolic heart failure workup." *World J. Methodol.* 7, 117–128 (2017).

[21]   Murphy, S. P., Ibrahim, N. E. & Januzzi, J. L., "Heart Failure with Reduced Ejection Fraction: A Review." *JAMA - J. Am. Med. Assoc.* 324, 488–504 (2020).

[22]   Kalogeropoulos, A. P. *et al.,* "Characteristics and outcomes of adult outpatients with heart failure and improved or recovered ejection fraction." *JAMA Cardiol.* 1, 510–518 (2016).

[23]   Chen, Y. T., Wong, L. L., Liew, O. W. & Richards, A. M., "Heart Failure with Reduced Ejection Fraction (HFrEF) and Preserved Ejection Fraction (HFpEF): The Diagnostic Value of Circulating MicroRNAs." *Cells* 8, 1–13 (2019).

[24]   Jenča, D. *et al.,* "Heart failure after myocardial infarction: incidence and predictors." *ESC Hear. Fail.* 8, 222–237 (2021).

[25]   Uriel, N., Sayer, G., Annamalai, S., Kapur, N. K. & Burkhoff, D., "Mechanical Unloading in Heart Failure." *J. Am. Coll. Cardiol.* 72, 569–580 (2018).

[26]   Gao, H. *et al.,* "Changes and classification in myocardial contractile function in the left ventricle following acute myocardial infarction." *J. R. Soc. Interface* 14, (2017).

[27]   Lorca, R. *et al.,* "Coexistence of transmural and lateral wavefront progression of

myocardial infarction in the human heart." *Rev. Española Cardiol. (English Ed.* 74, 870–877 (2021).

[28] Kuwada Y, Takenaka K., "Transmural heterogeneity of the left ventricular wall: subendocardial layer and subepicardial layer.". *J Cardiol.* 2000 Mar; 35(3):205-18.

[29] Delewi, R., Zijlstra, F. & Piek, J. J., "Left ventricular thrombus formation after acute myocardial infarction." *Heart* 98, 1743–1749 (2012).

[30] Kovačič, A. P. M. *et al.,* "Impact of drugs on venous thromboembolism risk in surgical patients." *Eur. J. Clin. Pharmacol.* 75, 751–767 (2019).

[31] Lopez-Perez, A., Sebastian, R. & Ferrero, J. M., "Three-dimensional cardiac computational modelling: METHODS, features and applications." *Biomed. Eng. Online* 14, 1–31 (2015).

[32] Trayanova, N. A. & Rice, J. J., "Cardiac electromechanical models: From cell to organ." *Front. Physiol.* 2 AUG, 1–19 (2011).

[33] Azevedo, P. S., Polegato, B. F., Minicucci, M. F., Paiva, S. A. R. & Zornoff, L. A. M., "Cardiac Remodeling: Concepts, Clinical Impact, Pathophysiological Mechanisms and Pharmacologic Treatment." *Arq. Bras. Cardiol.* 106, 62–69 (2016).

[34] Zhang, Z. *et al.,* "The benefit of enhanced contractility in the infarct borderzone: A virtual experiment." *Front. Physiol.* 3 APR, 1–6 (2012).

[35] Wenk, J. F. *et al.,* "Regional left ventricular myocardial contractility and stress in a finite element model of posterobasal myocardial infarction." *J. Biomech. Eng.* 133, (2011).

[36] Wang, H. *et al.,* "Computational Investigation of Transmural Differences in Left Ventricular Contractility." *J. Biomech. Eng.* 138, 1–6 (2016).

[37] Fan, L. *et al.,* "Material stiffness parameters as potential predictors of presence of left ventricle myocardial infarction: 3D echo-based computational modeling study." *Biomed. Eng. Online* 15, 1–16 (2016).

[38] Bassingthwaighte, J. B., Chizeck, H. J. & Atlas, L. E., "Strategies and tactics in multiscale modeling of cell-to-organ systems." *Proc. IEEE* 94, 819–830 (2006).

[39] Kerckhoffs, R. C. P., Narayan, S. M., Omens, J. H., Mulligan, L. J. & McCulloch, A. D., "Computational Modeling for Bedside Application." *Heart Fail. Clin.* 4, 371–378 (2008).

[40] Usyk, T. P., LeGrice, I. J. & McCulloch, A. D., "Computational model of three-

dimensional cardiac electromechanics." *Comput. Vis. Sci.* 4, 249–257 (2002).

[41] Shimkunas, R. *et al.,* "Left ventricular myocardial contractility is depressed in the borderzone after posterolateral myocardial infarction." *Ann. Thorac. Surg.* 95, 1619–1625 (2013).

[42] Kevin L. Sack1, Brian Baillargeon2, Gabriel Acevedo-Bolton3, Martin Genet3, 4, 5, N., Rebelo2, Ellen Kuhl6, Liviu Klein7, Georg M. Weiselthaler3, Daniel Burkhoff8, T. & Franz1, 9, and J. M. G., "Partial LVAD restores ventricular outputs and normalizes LV but not RV stress distributions in the acutely failing heart in silico." *Int J Artif Organs* 39, 421–430.

[43] Peskin CS., "Mathematical aspects of heart physiology." New York: Lecture Notes of Courant Institute of Mathematical Sciences; 1975

[44] Walker, J. C. *et al.,* "MRI-based finite-element analysis of left ventricular aneurysm." *Am. J. Physiol. - Hear. Circ. Physiol.* 289, 692–700 (2005).

[45] Shavik, S. M., Wall, S. T., Sundnes, J., Burkhoff, D. & Lee, L. C., "Organ-level validation of a cross-bridge cycling descriptor in a left ventricular finite element model: Effects of ventricular loading on myocardial strains." *Physiol. Rep.* 5, 1–14 (2017).

[46] Asner, L. *et al.,* "Patient-specific modeling for left ventricular mechanics using data-driven boundary energies." *Comput. Methods Appl. Mech. Eng.* 314, 269–295 (2017).

[47] Campos, R. S. *et al.,* "3D heart modeling with cellular automata, mass-spring system and CUDA." *Lect. Notes Comput. Sci. (including Subser. Lect. Notes Artif. Intell. Lect. Notes Bioinformatics)* 7979 LNCS, 296–309 (2013).

[48] Maurer, M. S. *et al.,* "Ventricular Structure and Function in Hypertensive Participants With Heart Failure and a Normal Ejection Fraction. The Cardiovascular Health Study." *J. Am. Coll. Cardiol.* 49, 972–981 (2007).

[49] Streeter, D. D., Spotnitz, H. M., Patel, D. P., Ross, J. & Sonnenblick, E. H., "Fiber orientation in the canine left ventricle during diastole and systole." *Circ. Res.* 24, 339–347 (1969).

[50] Triposkiadis, F. *et al.,* "Left ventricular geometry as a major determinant of left ventricular ejection fraction: physiological considerations and clinical implications." *Eur. J. Heart Fail.* 20, 436–444 (2018).

[51] Shavik, S. M. *et al.,* "Computational Modeling Studies of the Roles of Left Ventricular Geometry, Afterload, and Muscle Contractility on Myocardial Strains in Heart Failure

with Preserved Ejection Fraction." *J. Cardiovasc. Transl. Res.* 14, 1131–1145 (2021).

[52] Aikawa, T. *et al.,* "Impaired left ventricular global longitudinal strain is associated with elevated left ventricular filling pressure after myocardial infarction." *Am. J. Physiol. - Hear. Circ. Physiol.* 319, 1474–1481 (2020).

[53] Kasner, M., Sinning, D., Burkhoff, D. & Tschöpe, C., "Diastolic pressure–volume quotient (DPVQ) as a novel echocardiographic index for estimation of LV stiffness in HFpEF." *Clin. Res. Cardiol.* 104, 955–963 (2015).

[54] Gorcsan, J. & Tanaka, H., "Echocardiographic assessment of myocardial strain." *J. Am. Coll. Cardiol.* 58, 1401–1413 (2011).

[55] Hoit, B. D., "Strain and strain rate echocardiography and coronary artery disease." *Circ. Cardiovasc. Imaging* 4, 179–190 (2011).

[56] Smiseth, O. A., Torp, H., Opdahl, A., Haugaa, K. H. & Urheim, S., "Myocardial strain imaging: How useful is it in clinical decision making?" *Eur. Heart J.* 37, 1196-1207b (2016).

[57] Kraigher-Krainer, E. *et al.,* "Impaired systolic function by strain imaging in heart failure with preserved ejection fraction." *J. Am. Coll. Cardiol.* 63, 447–456 (2014).

[58] Li, S. *et al.,* "Comparison of Left Ventricular Global Strain in Anterior and Non-anterior Wall Myocardial Infarction With CMR Tissue Tracking." *Front. Physiol.* 11, 1–7 (2020).

[59] Bogaert, J. *et al.,* "Remote myocardial dysfunction after acute anterior myocardial infarction: Impact of left ventricular shape on regional function." *J. Am. Coll. Cardiol.* 35, 1525–1534 (2000).

[60] Bouchard, R. J., Gault, J. H. & Ross, J., "Evaluation of pulmonary arterial end-diastolic pressure as an estimate of left ventricular end-diastolic pressure in patients with normal and abnormal left ventricular performance." *Circulation* 44, 1072–1079 (1971).

[61] Masci, P. G. *et al.,* "Relationship between location and size of myocardial infarction and their reciprocal influences on post-infarction left ventricular remodelling." *Eur. Heart J.* 32, 1640–1648 (2011).

[62] Hirsch, G. A. *et al.,* "Age-related vascular stiffness and left ventricular size after myocardial infarction." *Am. J. Geriatr. Cardiol.* 16, 222–228 (2007).

[63] Brubakk, O. & Overskeid, K., "Systolic Time Intervals in Acute Myocardial Infarction." *Acta Med. Scand.* 199, 33–40 (1976).

[64]   Mangion, K., McComb, C., Auger, D. A., Epstein, F. H. & Berry, C., "Magnetic resonance imaging of myocardial strain after acute st-segment-elevation myocardial infarction a systematic review." *Circ. Cardiovasc. Imaging* 10, (2017).

[65]   Rajagopalan, V. *et al.,* "Safe oral triiodo-L-thyronine therapy protects from post-infarct cardiac dysfunction and arrhythmias without cardiovascular adverse effects." *PLoS One* 11, 1–16 (2016).

[66]   Elsman, P. *et al.,* "Impact of infarct location on left ventricular ejection fraction after correction for enzymatic infarct size in acute myocardial infarction treated with primary coronary intervention." *Am. Heart J.* 151, 1239.e9-1239.e14 (2006).

[67]   Thanavaro, S. *et al.,* "Effect of infarct location on the in-hospital prognosis of patients with first transmural myocardial infarction." *Circulation* 66, 742–747 (1982).

[68]   van Loon, T. *et al.,* "Increased myocardial stiffness more than impaired relaxation function limits cardiac performance during exercise in heart failure with preserved ejection fraction: a virtual patient study." *Eur. Hear. J. - Digit. Heal.* 1, 40–50 (2020).

[69]   Yamamoto, K. *et al.,* "Myocardial stiffness is determined by ventricular fibrosis, but not by compensatory or excessive hypertrophy in hypertensive heart." *Cardiovasc. Res.* 55, 76–82 (2002).

[70]   Leong, C. O. *et al.,* "Computational Modelling of the Effect of Infarct Stiffness on Regional Myocardial Mechanics." *Proc. Annu. Int. Conf. IEEE Eng. Med. Biol. Soc. EMBS* 6952–6955 (2019) doi:10.1109/EMBC.2019.8856771.

[71]   McComb, C. *et al.,* "Assessment of the relationships between myocardial contractility and infarct tissue revealed by serial magnetic resonance imaging in patients with acute myocardial infarction." *Int. J. Cardiovasc. Imaging* 31, 1201–1209 (2015).

[72]   Monge García, M. I. *et al.,* "Determinants of left ventricular ejection fraction and a novel method to improve its assessment of myocardial contractility." *Ann. Intensive Care* 9, (2019).

[73]   Michael R. Zile, William H. Gaasch, John D. Carroll, Marc D. Feldman, Gerard P. Aurigemma, Gary L. Schaer, Jalal K. Ghali, and P. R. L., "Heart Failure With a Normal Ejection Fraction." *J. Am. Hear. Assoc.* 104, 779–782 (2001).

NOMENCLATURE

HF	: Heart Failure
EF	: Ejection Fraction
HFrEF	: Heart Failure with reduced Ejection Fraction
HFpEF	: Heart Failure with preserved Ejection Fraction
ED	: End Diastole
ES	: End Systole
LV	: Left Ventricle
LA	: Left Atrium
RV	: Right Ventricle
RA	: Right Atrium
SL	: Semilunar Valve
HTN	: Hypertension
DD	: Diastolic Dysfunction
AV	: Atrioventricular Valve
SV	: Stroke Volume
MR	: Magnetic Resonance
ECG	: Electrocardiography
DBP	: Diastolic Blood Pressure
SBP	: Systolic Blood Pressure
ESPVR	: End-Systolic Pressure-Volume Relationship
EDPVR	: End-Diastolic Pressure-Volume Relationship
TPR	: Total Peripheral Resistance
Ees	: End Systolic Elastance